CHALMERS
UNIVERSITY OF TECHNOLOGY

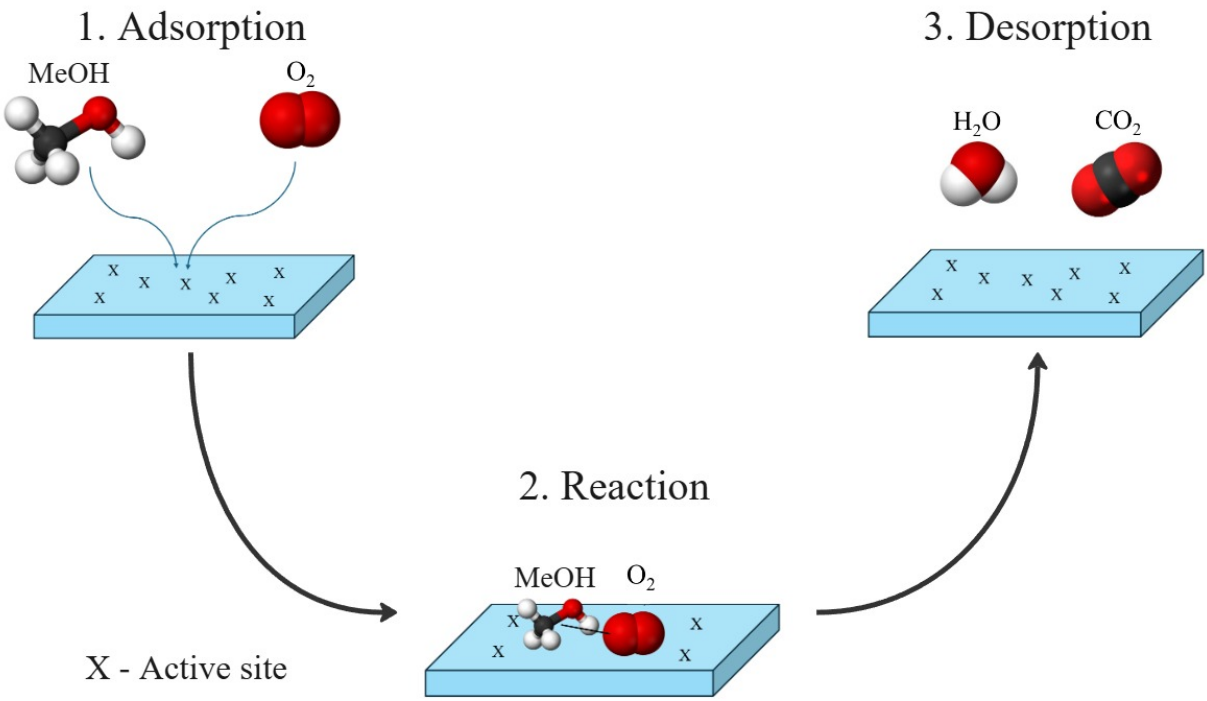

Development of a 1D Model for Methanol Engine Oxidation Catalyst

Methanol Oxidation Catalyst Modeling in GT-xCHEM

Master's thesis in Sustainable Energy Systems

GABRIEL LARSSON
ALEXANDER LINDHOLM

DEPARTMENT OF CHEMISTRY AND CHEMICAL ENGINEERING
CHALMERS UNIVERSITY OF TECHNOLOGY
Gothenburg, Sweden 2025
www.chalmers.se

Master's thesis 2025

Development of a 1D Model for Methanol Engine Oxidation Catalyst

Methanol Oxidation Catalyst Modeling in GT-xCHEM

GABRIEL LARSSON
ALEXANDER LINDHOLM

CHALMERS
UNIVERSITY OF TECHNOLOGY

Department of Chemistry and Chemical Engineering
Division of Chemical Engineering
Chalmers University of Technology
Gothenburg, Sweden 2025

Development of a 1D Model for Methanol Engine Oxidation Catalyst
Methanol Oxidation Catalyst Modeling in GT-xCHEM
GABRIEL LARSSON
ALEXANDER LINDHOLM

Supervisors: Wei Di, Chalmers University of Technology
Emma Westerborn, Volvo Penta
Julia Claesson, Volvo Penta
Mikael Nilsson, Volvo Penta
Examiner: Derek Creaser, Chalmers University of Technology

Master's Thesis 2025
Department of Chemistry and Chemical Engineering
Division of Chemical Engineering
Chalmers University of Technology
SE-412 96 Gothenburg
Telephone +46 31 772 1000

Cover: Stepwise illustration of methanol oxidation on a catalyst surface.

Typeset in LaTeX
Printed by Chalmers Reproservice
Gothenburg, Sweden 2025

Development of a 1D Model for Methanol Engine Oxidation Catalyst
Methanol Oxidation Catalyst Modeling in GT-xCHEM
GABRIEL LARSSON
ALEXANDER LINDHOLM
Department of Chemistry and Chemical Engineering
Chalmers University of Technology

Abstract

Developing an accurate 1D model of a methanol engine oxidation catalyst is an essential tool on the path towards sustainable transportation and emission control. The model could be used in early-stage development in order to evaluate feasibility and catalyst performance to shorten development time and reduce physical testing. Methanol is an alternative fuel that can be produced sustainably and has the potential of reducing some engine emissions such as nitrogen oxides (NO_x), sulfur oxides (SO_x) and soot, compared to conventional diesel. However it also results in some additional emissions in the form of formaldehyde and unburned methanol. It is therefore crucial to develop an effective methanol oxidation catalyst (MeOC), in which 1D modeling can be used as a key tool.

The aim of the study was to investigate if it is possible to successfully model a MeOC using GT-xCHEM. The method consisted of two main parts: synthetic gas bench (SGB) testing and modeling in GT-xCHEM. SGB testing was performed in order to calibrate, optimize and validate the model with experimental data. The optimization of the model was based on the results from the light-off temperature tests where the behavior of exhaust species were evaluated over a temperature range of 100-500 °C. Concentration scan tests were also done, in which steady-state results were obtained, which were later used to evaluate the model's accuracy. Finally, a scalability test was carried out, where the model was modified based on a full-scale catalyst, to assess the feasibility of scaling up the model. Formaldehyde, a species of interest, could unfortunately not be implemented in the study due to its instability.

From the results it could be concluded that it is possible to model a MeOC successfully in GT-xCHEM. It was found that the reactivity patterns of the species of interest: methanol (MeOH), carbon monoxide (CO), nitric oxide (NO) and nitrogen dioxide (NO_2) were interdependent on each other and the exhaust gas conditions. After optimization, the model correlated well with the experimental data gathered from the SGB tests, particularly for species MeOH, NO and NO_2. Furthermore, the scalability test proved that the model could be scaled up to model full-scale oxidation catalysts relatively well, even with some limitations in model setup. This clearly indicates the potential of using 1D modeling as a fundamental simulation tool. However, further refinement of the model is needed to better predict CO conversion and NO oxidation at high temperatures in order to accurately represent real-world conditions.

Keywords: Methanol, Catalyst, Modeling, Oxidation, Oxidation catalyst, Exhaust aftertreatment system

Acknowledgments

We would like to express our gratitude to our supervisors at Volvo Penta, Emma Westerborn, Mikael Nilsson and Julia Claesson, for their invaluable support and competent guidance throughout the duration of this project. Also, for giving us the opportunity to pursue this thesis work at Volvo Penta. Their support and encouragement have been instrumental for this thesis work. We would also like to extend our sincere thanks to Wei Di, our supervisor at Chalmers, for his creativity and technical assistance with the synthetic gas bench testing and test matrix development during challenging moments. His passion for research and his assistance in running tests has certainly enriched our experience. Additionally, we are grateful to Derek Creaser, our examiner, for his guidance and extensive knowledge of chemistry and chemical reaction engineering. His expertise particularly helped us with understanding the complex kinetic and inhibition dynamics in catalytic reactions as well as providing scientific explanations to our questions. Furthermore, we would like to acknowledge Lasse Urholm and Lennart Norberg at KCK for their tremendous support with laboratory equipment issues. Their ability to come up with new ideas and address our needs whenever challenges arose has been invaluable. Finally, we would like to thank Valesia Emmanouil and Dominik Artukovic at Gamma Technologies for their assistance in modeling and optimization issues in GT-xCHEM. Their role in this project has been crucial in enhancing our understanding of a software with which we had no prior experience with. Thank you all for your contributions to our master's thesis.

Gabriel Larsson and Alexander Lindholm, Gothenburg, June 2025

List of Acronyms

Below is the list of acronyms that have been used throughout this thesis listed in alphabetical order:

Ar	Argon
CCS	Carbon Capture and Storage
CO	Carbon monoxide
CO_2	Carbon dioxide
CS	Concentration Scan
DAC	Direct Air Capture
DF	Dual-Fuel
DOC	Diesel Oxidation Catalyst
EATS	Exhaust After Treatment System
FTIR	Fourier Transform Infrared Spectroscopy
GA	Genetic Algorithm
GHG	Greenhouse Gas
GT	Gamma Technologies
HCs	Hydrocarbons
HFO	Heavy Fuel Oil
H_2O	Water
LHV	Lower Heating Value
LNG	Liquefied Natural Gas
LOT	Light Off Temperature
MDO	Marine Diesel Oil
MeOC	Methanol Oxidation Catalyst
MeOH	Methanol
MGO	Marine Gas Oil
MS	Mass Spectrometer
N_2	Nitrogen gas
NO	Nitric oxide
NO_2	Nitrogen dioxide
NOx	Nitrogen oxides
O_2	Oxygen gas
PGM	Platinum Group Metal
PM	Particulate Matter
SCR	Selective Catalytic Reduction

Nomenclature

Below is the nomenclature of indices and parameters that have been used throughout this thesis.

Indices

30	Index for 30 % methanol conversion
80	Index for 80 % methanol conversion
eq	Index for equilibrium
exh	Index for exhaust
exp	Index for experimental
g	Index for gaseous phase
in	Index for catalyst inlet
j	Index for molar species
mol	Index for molecular
obj	Index for objective
out	Index for catalyst outlet
$pore$	Index for pore
$pred$	Index for predicted
w	Index for effective

Parameters

A	Pre-exponential factor
A_a	Adsorption pre-exponential factor
$\overline{C}_{g,j}$	Molar concentration of a specific specie in bulk gas
D_{knud}	Knudsen diffusion coefficient
D_{mol}	Molecular diffusion coefficient

D_w	Effective diffusion coefficient
d_{pore}	Mean pore diameter
E	Total internal energy of bulk gas
E_i	Activation energy for species i
E_a	Adsorption activation energy
F_{obj}	Transient targeting objective function
G	Inhibition term
H	Total enthalpy of bulk gas
k	Kintic rate constant
K'	Deviation from equilibrium
K_{eq}	Equilibrium constant
$\dot{m}$	Mass flow
M	Molar mass
p	Pressure of bulk gas
r	Reaction rate
R	Universal gas constant
S	Source term
t	Time
T	Temperature
u	Velocity of bulk gas
x	Axial distance
X	Output or reference value from transient targeting optimization
ε_{pore}	Pore porosity
ρ_g	Density of bulk gas
τ	Tortuosity

Contents

List of Figures

List of Tables

1

Introduction

The following chapter provides an introduction to the Master's thesis, including Background, Aim, Limitations, and Specification of the Issue Being Investigated.

1.1 Background

The transportation sector is at the core of today's society which provides possibilities for meetings between people, as well as trade of goods around the world. Transportation by sea is a major contributor with around 80 % of all traded volume carried by sea [2]. In 2018, the maritime transport and inland navigation sector contributed to 13.5 % of the EU's total transportation greenhouse gas (GHG) emissions [3]. Developing sustainable solutions for the maritime sector is therefore crucial for reducing GHG emissions. Volvo Penta has made a commitment to reduce CO_2 emissions as one of the world's leading suppliers of marine engines. Methanol engines can play a crucial role in this commitment, depending on the production path. The marine engines are equipped with an Exhaust Aftertreatment System (EATS), which today primarily consists of a Selective Catalytic Reduction (SCR) unit, designed to reduce NO_x emissions.

Diesel is widely used in marine engines due to its reliability and high efficiency [4]. Combustion of diesel produces exhaust gases containing substances like nitrogen oxides (NO_x), carbon monoxide (CO), hydrocarbons (HCs) and particulate matter (PM) which are harmful to both humans and the environment. However, NO_x is the primary emission of concern in today's legislation and is reduced to minimize the human- and environmental impact as well as comply with legal requirements.

A way of further reducing these emissions is to use alternative fuels like methanol in combination with an EATS. One form of methanol is e-methanol, which is a promising fuel, that is expected through its life cycle to become accepted as a carbon neutral fuel due to advanced carbon capture and methanol synthesis [5]. Bio-methanol is also a promising option, as methanol is produced using syngas obtained from gasification or reforming of biogenic carbon feedstock [6]. Regardless of the fuel origin, the EATS for a methanol marine engine will require the addition of an oxidation catalyst due to high emissions of hydrocarbons, carbon monoxide and the formation of formaldehyde, when compared to diesel engines [4].

One-dimensional (1D) models can be used to simulate systems and give a holistic

view and understanding of how different components interact with each other [7]. Components are mapped out and connected to simulate flows in a real-life system. Properties and specifications are applied to each component based on their physical properties. Laboratory testing can then be used as a tool to improve the 1D modeling software's understanding of each component. With a satisfactory model, physical testing can be complemented with or replaced by computational simulations, thereby saving both time and resources.

Dual-fuel diesel–methanol and 100 % methanol marine engines show great promise in reducing NO_x and soot emissions [4]. However, the introduction of methanol as an additional fuel to the engine will result in some new emissions, compared to a conventional diesel engine, such as unburned methanol and formaldehyde. Therefore, developing an effective methanol oxidation catalyst (MeOC) is of great importance. An 1D model of the catalyst can provide insight into how the MeOC performs under different operating conditions, as well as how the EATS should be designed to meet legal requirements and reduce harmful emissions.

1.2 Aim

The aim of this master's thesis is to develop a 1D model for a methanol oxidation catalyst using GT-xCHEM. SGB testing will be performed to calibrate the model and supply it with supporting data. The desire is that the model can be scalable and applicable on full-scale oxidation catalysts for methanol engines constructed by Volvo Penta on their journey towards sustainable transportation.

1.3 Limitations

Identified limitations with regard to the scope of the thesis are presented in the form of bullet points.

- The model will be based on a laboratory-scale rig that does not have exactly similar properties, for example space-velocity, as a large-scale marine methanol engine.
- The SGB cannot fully simulate all of the exhaust gas species concentrations due to technical constraints and availability of gases.
- Formaldehyde, a species of interest, cannot be measured during the experiments because the equipment cannot be calibrated for it, primarily due to its low boiling point and chemical instability.
- Full-scale oxidation catalyst test data, which will be used for a scalability test, only exists for a dual-fuel engine and not for 100 % methanol.

1.4 Specification of the Issue Being Investigated

The study aims to address multiple questions essential for the design and introduction of an effective methanol oxidation catalyst. Key questions include:

- Is it possible to model a MeOC successfully using SGB testing and GT-xCHEM?
- What is the feasibility of scaling the model to function effectively on full-sized dual-fuel methanol-diesel, or 100 % methanol, engines?
- How does the methanol oxidation catalyst perform under varying operating conditions?
- What are the interactions between the different species of interest, and how are their behaviors interdependent during the given conditions?

2

Theory

A chapter containing the theoretical background and knowledge that is fundamental for understanding the thesis.

2.1 Exhaust Aftertreatment System (EATS)

The exhaust gases formed in the engine are transported to an exhaust aftertreatment system (EATS) primarily designed to reduce NO_x [8]. Marine EATS typically consists only of a SCR, due to NO_x being the main emission of legal concern from marine diesel systems. An illustrative representation of current marine EATS can be seen in Figure 2.1a. Alternative fuels are likely to be implemented in the future due to the growing emphasis on climate change mitigation. As a result of this, marine EATS, depending on the fuel, will likely include more advanced components in the future. An oxidation catalyst is one example of an additional component that can be used to fully oxidize exhaust gases. It becomes necessary when emissions such as unburned HCs, CO, and other products of incomplete combustion are formed. Methanol is an example of a fuel that would require the use of an oxidation catalyst. A potential future EATS including an oxidation catalyst can be seen in Figure 2.1b.

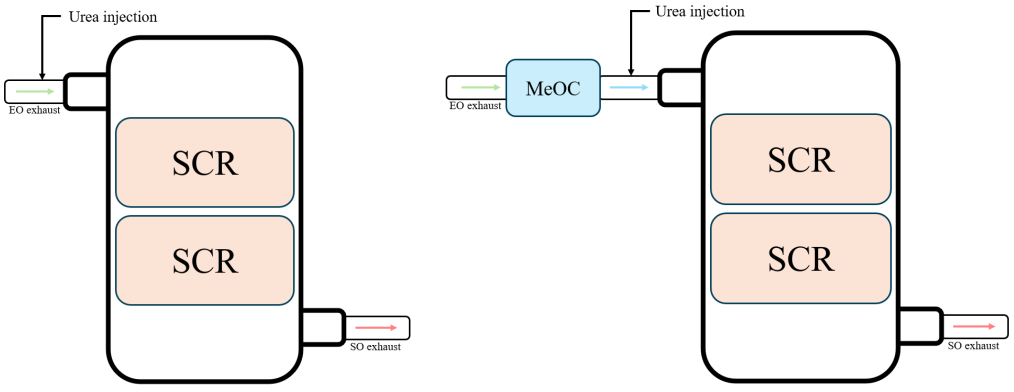

Figure 2.1: Illustration of (a) today's marine EATS and (b) future marine EATS.

Figure 2.1a shows how urea is injected into the exhaust gas flow through an injector to be able to reduce NO_x later in the SCR [9]. NO_x reacts in various ways in the

SCR, forming N_2 and water (H_2O)[10].

2.1.1 Oxidation Catalyst

The oxidation catalyst, a component of future EATS, reduces harmful emissions by oxidizing HCs, NO_x and CO into less harmful products [11]. The structure of the oxidation catalyst is generally based on cordierite (ceramic) monoliths with low porosity and therefore excellent strength. This ceramic structure is coated with a washcoat where precious metals with catalytic properties are dispersed. The monolith has a "honeycomb" structure with multiple small channels, maximizing surface area for the oxidation reactions to occur. The high surface area and even dispersion of active material increases the oxidation efficiency as well as reduces the amount of metals needed, resulting in lower total catalyst cost. An illustration of a general structure can be seen in Figure 2.2.

Thermal aging of oxidation catalysts is a typical phenomenon affecting oxidation catalysts during their lifetime. The catalyst activity decreases slightly under high temperatures, primarily through sintering of both the platinum group metals (PGMs) and the washcoat material [12]. The process causes smaller PGM particles to agglomerate into larger ones which subsequently decreases the catalytic surface activity. If the washcoat undergoes sintering, the structure of the monolith can collapse which can encapsulate PGMs, further decreasing the activity of the catalyst.

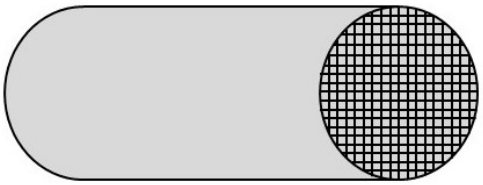

Figure 2.2: Schematic picture of a monolithic oxidation catalyst.

2.1.1.1 Methanol Oxidation Catalyst (MeOC)

To address the additional emissions from methanol combustion, a methanol oxidation catalyst must be developed. The MeOC is placed upstream of the SCR in the marine EATS and is designed to reduce harmful emissions [13]. The concentration of CO, NO_x, formaldehyde and unburned methanol will vary depending on the proportion of methanol in the fuel. The reaction mechanism for CO, HCs and NO_x will be further described in Section 2.1.1.2.

The precious metals in the MeOC work as catalysts for the oxidation reactions. Methanol is both partially and completely oxidized in the catalyst, which can be seen in Reaction R1-R2. Partial oxidation of methanol is noted because it leads to formaldehyde formation. However, it will unfortunately not be further discussed in this work, nor included in the model, due to the limitations of formaldehyde detection in the SGB rig.

$$CH_3OH + \frac{1}{2}\,O_2 \longrightarrow CH_2O + H_2O \tag{R1}$$

$$CH_3OH + \frac{3}{2}\,O_2 \longrightarrow CO_2 + 2\,H_2O \tag{R2}$$

The presence of a MeOC helps decrease the formaldehyde (CH_2O) emissions through oxidation, the two main reactions can be seen in Reaction R3-R4 [14]. The MeOC can either reduce the amount of formaldehyde in the exhaust gases or it could favor the production of formaldehyde, depending on the exhaust gas temperature.

$$CH_2O + \frac{1}{2}\,O_2 \longrightarrow HCOOH \tag{R3}$$

$$CH_2O + O_2 \longrightarrow CO_2 + H_2O \tag{R4}$$

2.1.1.2 Reaction Mechanisms

The most widely accepted mechanism for CO oxidation is the Langmuir-Hinshelwood dual-site mechanism [11]. This reaction mechanism is illustrated in Reaction R5-R7, where * represents a vacant active site at the catalyst surface. Reactions R5 and R6 describe how CO and O_2 adsorb onto vacant sites on the catalyst surface. CO molecules have the ability to migrate across the catalyst surface, interact with oxygen, and react to form CO_2, which afterward desorb from the active sites. This can be seen in Reaction R7.

$$CO + {}^\star \rightleftharpoons CO^\star \tag{R5}$$

$$O_2 + 2\,{}^\star \rightleftharpoons 2\,O^\star \tag{R6}$$

$$O^\star + CO^\star \longrightarrow CO_2 + 2\,{}^\star \tag{R7}$$

Unburned HCs are also oxidized in the MeOC according to the Langmuir-Hinshelwood dual-site mechanism [11]. The reaction mechanism can be seen in Reaction R8-R10, where $^¤$ and * represent different active sites. Reaction R8 describes how oxygen adsorb onto an active site and later split into two oxygen atoms onto two different

sites. Reaction R9 describes how a HC adsorb onto another vacant site and then Reaction R10 illustrates a unbalanced reaction between a general HC and oxygen to form CO_2, which afterward desorb from the vacant site. Since methanol is less extensively studied, it is assumed to follow the same reaction pathway as other HCs.

$$O_2 + {}^\star \longrightarrow O_2{}^\star \longrightarrow 2\,O^\star \tag{R8}$$

$$HC + {}^¤ \rightleftharpoons HC^¤ \tag{R9}$$

$$HC^¤ + O^\star \longrightarrow CO_2 + {}^\star + {}^¤ \tag{R10}$$

The general reaction of NO and NO_2 can be seen in Reaction R11-R14. Reaction R11 describes how NO absorb onto a vacant site and Reaction R12 describes how NO_2 absorb onto the surface, breaks apart, and forms NO and O at the surface. Reactions R13-R14 describe how oxygen absorbs onto the catalyst surface and then splits into two oxygen atoms at one site each.

$$NO + {}^\star \rightleftharpoons NO^\star \tag{R11}$$

$$NO_2 + 2\,{}^\star \rightleftharpoons NO^\star + O^\star \tag{R12}$$

$$O_2 + {}^\star \longrightarrow O_2{}^\star \tag{R13}$$

$$O_2{}^\star + {}^\star \longrightarrow 2\,O^\star \tag{R14}$$

2.2 Marine Fuels

Since the beginning of the marine industry, fuel use has been predominantly fossil-based, including heavy fuel oil (HFO), marine gas oil (MGO) and marine diesel oil (MDO) [15]. Due to growing concerns about climate change, efforts have shifted towards more environmentally friendly alternative fuels, some examples are liquefied natural gas (LNG), hydrogen, biofuel, ammonia (NH_3) and methanol. The main benefit of alternative fuels is their potential to reduce GHG emissions. Some, such as hydrogen and ammonia, have the benefit of not producing any direct carbon emissions, while others main advantage is that they can be produced in a sustainable way, for example biofuel and methanol. Methanol is the focus of this study, including the potential of using it in dual-fuel systems alongside diesel.

2.2.1 Diesel

As previously mentioned, diesel in its various forms has been the predominant fuel type for marine applications, alongside HFO [15]. This section outlines the key characteristics and properties of diesel, its production methods and lastly the emissions associated with its use in diesel engines.

2.2.1.1 Characteristics

In marine contexts, the term "diesel" can be used as a collective name for both MGO and MDO. MGO is essentially identical to the diesel used in automotive engines, while MDO on the other hand contains a mixture of HFO and MGO [16]. Diesel-fueled engines are widely used in marine applications due to their high efficiency and realiability.

2.2.1.2 Production

Diesel is primarily produced by refining petroleum crude oil into a distillate of hydrocarbons with carbon-chain lengths ranging from C_{10} to C_{15}. However, it is also possible to produce diesel from a non-fossil feedstock, for example renewable diesel or bio-diesel which is produced from a bio-based feedstock [17]. Renewable diesel is chemically equivalent to fossil diesel and can be used as a direct substitute or blended with petroleum diesel. Bio-diesel is another sustainable alternative to diesel that is produced through transesterification of vegetable oils and animal fats.

2.2.1.3 Emissions

Emissions from diesel combustion include gaseous, liquid and solid pollutants that are harmful to both human health and the environment [11]. Gaseous compounds of concern are carbon monoxide, unburned hydrocarbons, nitrogen oxides and carbon dioxide. Particulate matter is the main solid compound that is formed and can pose serious health risks. Incomplete combustion of the fuel is the main reason behind emissions, which results in CO, HCs and soot formation. Ideally, complete combustion is desired, which only results in H_2O and CO_2 being formed.

Diesel engines are operated with a lean mixture of fuel and air, which means that fuel is injected into an excess amount of compressed air to achieve combustion. The high air-to-fuel ratio is one of the reasons why NO_x emissions are a substantial concern in diesel engines since it makes the reduction of NO_x to N_2 much more difficult. Most of the nitrogen oxides in the exhaust of an engine come from thermal NO_x, which is formed when nitrogen and oxygen in the air are combined during combustion at very high temperatures. Additionally, a small part of the exhaust NO_x is formed when fuel-bound nitrogen is oxidized. To reduce NO_x emissions, ammonia containing urea is injected into the exhaust in the SCR, resulting in an additional emission in the form of unreacted NH_3.

2.2.2 Methanol

Methanol is an alternative fuel that shows great potential since it has the possibility to reduce the emissions of NO_x and soot from diesel engines [4]. It also has the great benefit that it could be produced sustainably in the form of either e-methanol or bio-methanol [15]. This will be discussed further in this section as well as the characteristics, production and emissions related to methanol combustion.

2.2.2.1 Characteristics

Methanol is an alcohol and has a chain-length of only one carbon atom. It is entirely sulfur-free, with the right feedstock, which is beneficial to avoid corrosion, catalyst poisoning, health, and environmental complications [18]. Compared to diesel it is less energy dense, diesel has a lower heating value (LHV) that is double the one of methanol. This means that either the fuel storage infrastructure must be expanded or that the fuel range must be reduced. Another great benefit of methanol for maritime applications is its water solubility and biodegradability, in case of fuel spillage [6]. Additionally, methanol is easy to store and transport since it is a liquid at ambient conditions. The availability is also an advantage since it is a widely used chemical and that industrial scale production is already in place. However, most of the methanol production is currently from fossil-carbon feedstock.

2.2.2.2 Production

The production of methanol is today mostly from fossil-based carbon feedstock, such as carbon and natural gas [6]. However, it is also possible to produce methanol from other carbon containing feedstock such as biomass, waste, biogas and CO_2. The two main types of sustainable methanol are bio-methanol and e-methanol. Bio-methanol is produced from gasification or by reforming of a biogenic feedstock, for example forestry and agricultural waste, biogas or black liquor from the pulp industry.

Green e-methanol is another sustainable production route that has been identified. It consists of synthesizing methanol from CO_2 and hydrogen produced from water electrolysis, ideally using electricity from renewable energy sources [19]. However, production of e-methanol is highly energy intensive, expensive, and also limited to the availability of green electricity. How CO_2 is sourced is also an important aspect to consider with Direct Air Capture (DAC) and Carbon Capture and Storage (CCS) being the most suggested technologies. However, both technologies are energy-intensive, expensive and still at an early stage of implementation.

2.2.2.3 Emissions

Combustion of methanol results in some additional emissions, compared to conventional diesel combustion, which are formaldehyde and unburned methanol. When it comes to more conventional emissions, there is a drastic change in particulate matter emissions due to methanol not being a long-chain hydrocarbon [20]. It also has a high H/C ratio, and some studies have found that with similar engine efficiencies it emits 20 % less CO_2 than diesel during combustion [20]. Since methanol is oxy-

genated, with an oxygen content of 50 wt%, combustion is more efficient, requires less air, and results in reduced soot emissions. Additionally, a lower combustion temperature is achieved with methanol compared to diesel, which in turn results in less NO_x formation. Also, since it can be an entirely sulfur-free fuel, sulfur oxides (SO_x) can be avoided in the exhaust, although ultra low sulfur diesel is achievable with the right production and cleaning method [21].

However, studies have found that emissions of HC and CO increase when methanol is used as fuel, compared to conventional diesel [4]. Aldehyde emissions occur due to incomplete combustion of methanol, especially prominent during cold start, and are species that is not commonly found in diesel engine exhaust. Lastly, the introduction of another new emission compound in the form of unburned methanol, promotes the development of a more specialized methanol oxidation catalyst, see Section 2.1.1.1.

2.2.3 Dual-Fuel Systems

Dual-fuel (DF) systems utilize two fuels instead of one, diesel-methanol DF engines have been gaining increasing interest due to the technical challenges in developing neat methanol combustion engines [4]. Also, due to the already existing diesel dominated infrastructure. Dual-fuel systems offer an alternative by partially substituting diesel and subsequently reducing harmful NO_x and soot emissions. This could be done either by premixing diesel and methanol or by injecting methanol into the air intake, two measures that can both be applied to existing diesel engines. As for the premixing case, since diesel and methanol have poor miscibility an additive is required to ensure proper mixing before engine injection [4].

In the other alternative, sometimes called the fumigation approach, methanol and diesel are injected separately [4]. The conventional fuel injector supplies the engine with diesel and methanol is injected through the air intake. The fumigation method has been shown to allow for more operational flexibility and higher methanol fractions in the engine. A major drawback with using a dual-fuel system is the high aldehyde emissions during cold start along with the difficulty in engine start-up. This issue can be mitigated by employing a system that only uses diesel during start-up to avoid incomplete combustion of methanol, a system that could potentially require diesel engine retrofitting.

2.3 Modeling

Modeling is a tool that contributes to the development of new technology, in this case, a methanol oxidation catalyst. The development of mathematical models of catalysts such as a MeOC is crucial for improving the efficiency and control while minimizing time and cost of experimental tests [22].

2.3.1 1D Modeling

The optimal mathematical model for predicting the catalytic performance would be three-dimensional (3D) as the actual flow occurs in all three dimensions [22].

However, modeling the conversion and temperature profiles for all channels in 3D is complex as well as computationally heavy. In addition, all the kinetics would be difficult to model accurately and would still require calibration from experimental data. Therefore, a one-dimensional model is a better option due to its computationally efficiency, relatively accuracy, and ease of calibration.

2.3.1.1 Conservation equations

The 1D approach of solving reacting flows in channels is based on the conservation of mass, momentum, energy, and molar species. These conservation equations, including generalized source terms, are defined in Equations 2.1-2.4 [22].

$$\frac{\delta \rho_g}{\delta t} + \frac{\delta(\rho_g u)}{\delta x} = S_{\text{mass}} \tag{2.1}$$

$$\frac{\delta(\rho_g u)}{\delta t} + \frac{\delta(\rho_g u^2 + p)}{\delta x} = S_{\text{momentum}} \tag{2.2}$$

$$\frac{\delta(\rho_g E)}{\delta t} + \frac{\delta(\rho_g u H)}{\delta x} = S_{\text{energy}} \tag{2.3}$$

$$\frac{\delta \overline{C}_{g,j}}{\delta t} + \frac{\delta(u\overline{C}_{g,j})}{\delta x} = S_j \qquad j = 1, ..., \text{NM} \tag{2.4}$$

2.3.1.2 Reactions and Kinetics

Several reactions are presumed to take place in a MeOC. The ones considered most prominent, and thus studied within the scope of this project are shown in Reactions R15–R19.

$$\text{CO} + \frac{1}{2}\,\text{O}_2 \longrightarrow \text{CO}_2 \tag{R15}$$

$$\text{NO} + \frac{1}{2}\,\text{O}_2 \rightleftharpoons \text{NO}_2 \tag{R16}$$

$$\text{MeOH} + \frac{3}{2}\,\text{O}_2 \longrightarrow \text{CO}_2 + 2\,\text{H}_2\text{O} \tag{R17}$$

$$\text{CO} + \text{NO}_2 \longrightarrow \text{CO}_2 + \text{NO} \tag{R18}$$

$$\mathrm{MeOH} + 3\,\mathrm{NO_2} \longrightarrow \mathrm{CO_2} + 3\,\mathrm{NO} + 2\,\mathrm{H_2O} \tag{R19}$$

Catalysts are used to change the rate of a chemical reaction by lowering the activation energy [23], [24]. The kinetic rate constant can be expressed by the Arrhenius equation as shown in Equation 2.5.

$$k_i = A_i \exp\left(\frac{-E_i}{RT}\right) \tag{2.5}$$

Where k_i is the kinetic rate constant for species i, A_i is the pre-exponential factor, E_i is the activation energy, R is the universal gas constant and T is the temperature. The reaction rate is thus given by the product of the reaction rate constant and the species concentration. Equations 2.6–2.10 shows the reaction rate for CO, CH_3OH and NO oxidation, with both O_2 and NO_2 as oxidizing agents [25] [26]. Equation 2.7 is slightly different from the other reaction rates since it contains both kinetic and thermodynamic considerations. This is because NO oxidation is influenced by NO_2 self-dissociation at high temperatures. Therefore, an additional term containing the equilibrium constant is included, where K' represents how the mixture deviates from equilibrium and its expression is given in Equation 2.12. K_{eq} denotes the equilibrium constant and is derived from the standard Gibbs free energy of NO oxidation, the resulting expression can be seen in Equation 2.11 [1].

$$r_{R15} = \frac{k_{R15}\,[\mathrm{CO}]\,[\mathrm{O_2}]^{1/2}}{G} \tag{2.6}$$

$$r_{R16} = \frac{k_{R16}[\mathrm{NO}][\mathrm{O_2}]^{1/2}}{G}\left(1 - \frac{K'}{K_{eq}}\right) \qquad K' < K_{eq} \tag{2.7}$$

$$r_{R17} = \frac{k_{R17}\,[\mathrm{CH_3OH}]\,[\mathrm{O_2}]^{1/2}}{G} \tag{2.8}$$

$$r_{R18} = \frac{k_{R18}\,[\mathrm{CO}]\,[\mathrm{NO_2}]}{G} \tag{2.9}$$

$$r_{R19} = \frac{k_{R19}\,[\mathrm{CH_3OH}]\,[\mathrm{NO_2}]}{G} \tag{2.10}$$

$$K_{eq} = 1.5 \cdot 10^{-4} \exp\left(6864/T\right) \tag{2.11}$$

$$K' = \frac{X_{\mathrm{NO_2}}}{X_{\mathrm{NO}} X_{\mathrm{O_2}}^{1/2}} \tag{2.12}$$

Where G represents the combined inhibition expression for all species, described in Section 2.3.1.3.

2.3.1.3 Inhibition

The reaction rate can also be limited by inhibition between reactants, where species compete with each other for active sites on the catalyst surface which is represented by G in the reaction rate term. The inhibition term is defined in Equation 2.13 [26].

$$G = \left[1 + A_{a_{\mathrm{CO}}} \exp\left(\frac{-E_{a_{\mathrm{CO}}}}{R_g T_s}\right)[\mathrm{CO}] + A_{a_{\mathrm{CH_3OH}}} \exp\left(\frac{-E_{a_{\mathrm{CH_3OH}}}}{R_g T_s}\right)[\mathrm{CH_3OH}] + A_{a_{\mathrm{NO}}} \exp\left(\frac{-E_{a_{\mathrm{NO}}}}{R_g T_s}\right)[\mathrm{NO}]^{0.7}\right]^2 \tag{2.13}$$

Where A_{a_i} is the pre-exponential adsorption factor and E_{a_i} represents the adsorption activation energy of each individual species. These parameters depend on both the conditions and the catalyst used for a specific reaction. Some reference values have been compiled in Table 2.1 that have been widely established for modeling automotive catalysts [25]. The kinetic parameters for methanol adsorption have not been thoroughly investigated and therefore, the parameters has been estimated based on short-chain hydrocarbons (C_3H_6) [26].

Table 2.1: Reference inhibition parameters for CO, CH_3OH and NO adsorption.

Parameter	**CO**	**CH_3OH**	**NO**
Pre-exponential factor (A_{a_i}) [-]	65.5	$2.5 \cdot 10^2$	$4.79 \cdot 10^5$
Activation energy/R_g (E_{a_i}/R_g) [K]	-961	-750	3733

2.3.2 Optimization and Calibration

The model needs to be calibrated to improve the accuracy since the 1D model is a representation of a 3D system [22]. Optimization and calibration are crucial steps in modeling to ensure that the model accurately reflects reality. This is done by using experimental data to improve parameters, like kinetic rate expressions as well as inhibition parameters. This optimization of the model will increase the accuracy and predict the experimental results more effectively. Activation energy and other important reaction properties are obtained by combining experimental testing with research through chemical databases and other relevant literature.

2.3.2.1 Genetic Algorithm (GA)

A genetic algorithm is a tool that can be used to optimize and calibrate a model. Natural selection has given inspiration to genetic algorithms, which are a type of search algorithm [27]. They utilize the "survival of the fittest" principle from natural selection and apply it to search algorithms. This is done through multiple generations of different populations of individuals and by analyzing which of these individuals that have the best chance of survival or for search algorithms, which individuals represent the best solutions.

A simple genetic algorithm consists of three steps: (1) Reproduction, the best population groups from the first generation reproduce to carry over the best solutions from the first generation to the second, the rest of the individuals are discarded; (2) Crossover/recombination, a process in which two selected individuals combine and produce an even better solution; (3) Mutation, small random changes are made to some populations to discover new areas of the search domain, to avoid converging toward local optima [27]. In this way, GAs are not random-walk search algorithms, rather they utilize historic events to predict new search points. The user can define how many generations are to be generated or continue the optimization process until the user is satisfied with the solution. The solution is constantly improved with each generation, with the end-goal of finding an optimum.

For the search algorithm to be able to determine the best possible solution, each design iteration is evaluated using a transient targeting objective function. The expression that is utilized in GT-xCHEM can be seen in Equation 2.14. In this expression, i represents a certain species and n is the number of species investigated in the optimization. The objective function computes the squared error between the predicted and experimental results, meaning that the target is to achieve a value as close to zero as possible.

$$F_{obj} = \int_{t_0}^{t} \sum_{i=1}^{n} \left(X_{i,pred} - X_{i,exp}\right)^2 \tag{2.14}$$

3

Methodology

This chapter contains the structure and overall workflow of the thesis, including how the testing, modeling and optimization were carried out.

3.1 SGB Testing

SGB testing was performed in order to gather experimental data for model calibration and optimization. The procedure will be described in more detail in this chapter.

3.1.1 Test Matrix and Planning

The test matrix planning is a crucial part of the SGB testing procedure to ensure that the tests are representative of real engine emissions. The test matrix included two types of tests: A light-off temperature test (LOT) and a concentration scan (CS) test. The idea was that these tests could give a variation in results that could be used for calibration and validation of the model later in the project.

3.1.2 Sample Preparation

After the test matrix had been constructed, sample preparations were performed. A large-scale Pt/Pd oxidation catalyst with 400 CPSI was delivered from an external supplier, which can be seen in Figure 3.1. The catalyst was then cut horizontally into four discs with a height of 16 mm each in order to get the desired length of the catalyst.

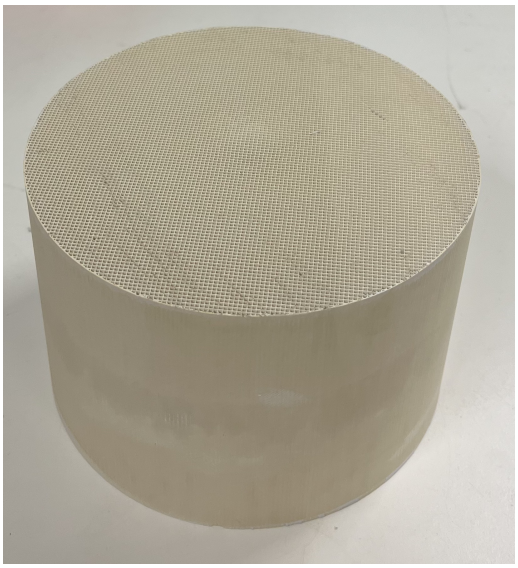

Figure 3.1: Catalyst provided from supplier.

The catalyst samples were then cut out from the middle of each disc in a honeycomb shape with a diameter of 16 millimeters to fit inside the reactor setup. This was done by removing the outer channels, one by one with a knife, until the desired shape of the catalyst was achieved. Two samples were prepared: one designated as the main catalyst and the other as a spare, intended for use in case the first sample was damaged. The samples were taken from the middle of the catalyst, as this region was assumed to have the most uniform coating. Figure 3.2 shows the end-result of the sample after cutting. After the catalysts had been cut out they were thermally aged in an oven at 700 °C for 20 hours. This was done to get more realistic results of how a catalyst performs in actual engine conditions.

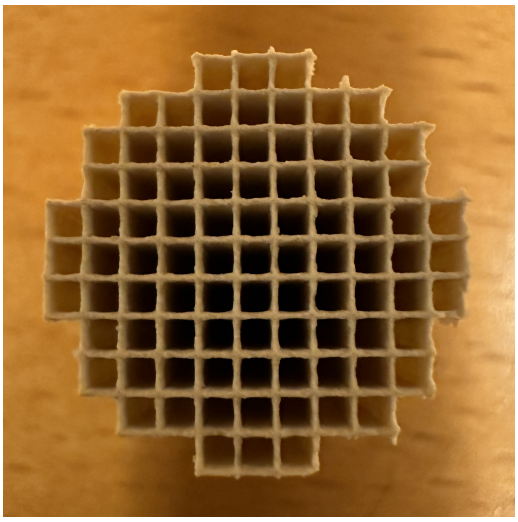

Figure 3.2: An image of the catalyst sample used for laboratory testing after cutting.

3.1.3 SGB Reactor Setup

The SGB reactor consisted of a quartz glass tube with the catalyst sample placed inside. Quartz wool was used as insulation material, wrapped around the quartz reactor, to minimize heat losses and maintain thermal stability throughout the experiments. The gas mixture was first pre-heated before it entered the reactor, in which it was further heated up to the desired reactor temperature. Electric heat was supplied to the reactor through a spiral coil and there were two thermocouples, one before the catalyst sample and one close to the catalyst. The gas flow was then fed through a Fourier Transform Infrared Spectroscopy (FTIR) and a Mass Spectrometer (MS) after the catalyst, to monitor the composition of the gas. Methanol and water was supplied through a separate liquid system that was used to evaporate the two liquids before being mixed with the other gases. The system consisted of a small storage tank, an evaporator and a mass flow controller along with a carrier gas, in the form of inert argon, which transported the vaporized liquids. Figure 3.3 provides a holistic view of the reactor setup in its entirety.

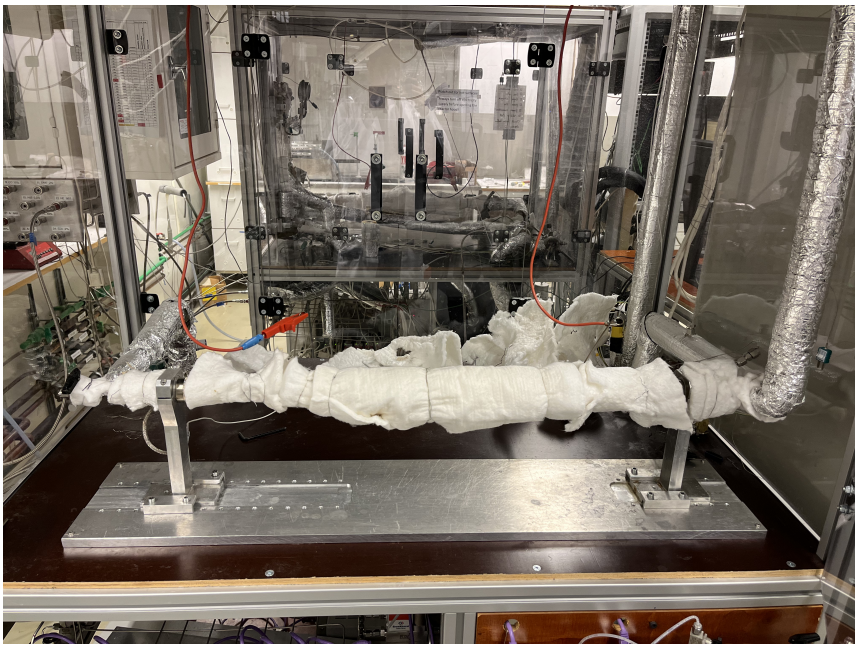

Figure 3.3: Overview of the SGB reactor setup.

3.1.4 Calibration of Measuring Equipment

To ensure that the right concentrations are used in the experiments and that the FTIR and MS measurements were correct, calibration of both devices was performed. The calibration was done in two batches, one with the liquids (MeOH and H_2O) and one with the gases (CO, NO, NO_2, O_2, CO_2 and Ar). The liquid calibration is of great importance to determine the specific mass flow rate that represents a certain concentration. Therefore, three operating points were explored to find the actual concentrations. Afterwards, regression could be used to find the correct dependency between mass flow rate and measured concentration.

3.1.5 Pre-Conditioning

To ensure that each test was performed under similar conditions, the catalyst samples were pre-conditioned with the same procedure each time. The pre-conditioning consisted of the following steps:

1. **High temperature pre-conditioning with O_2:** Fully oxidized the catalyst surface. Carried out at 450 °C for 5 minutes.
2. **Cool-down in presence of Ar:** The oxidation catalyst was cooled down to the desired start temperature of each test.
3. **H_2O/CO_2 exposure:** Saturation of oxidation catalyst with H_2O and CO_2 prior to the test, in order to avoid competing mechanisms with methanol.

3.1.6 LOT Test

The first step of the SGB testing was to perform a LOT test. This test was used to determine at which temperature the catalyst becomes active and as reference data for later calibrating the kinetic parameters in the model. This was done by gradually ramping up the temperature with a rate of 5 °C/min from 100 to 500 °C while the concentration of MeOH, CO, NO, NO_2 was monitored. Testing was done with various exhaust gas compositions to see how the LOT was affected under different conditions. The LOT could afterwards be determined at the temperature at which the concentration of a certain species starts to decrease, in other words when the conversion of the same species starts to increase. The composition of the LOT tests is described by the test matrix shown in Table 3.1. The idea was to vary the concentration of one species at a time to see how it impacts the overall reactions inside the catalyst. Also, with the intention of making a versatile model that can be applicable in several operating conditions. The ratios between the species were based on real engine-out data provided by Volvo Penta, to make the synthetic gas representable of actual engine exhaust gas. The concentration of O_2 was kept constant at an excess amount of 8 %. The concentration of H_2O and CO_2 was also kept constant since they are not of interest due to them already being fully oxidized.

Table 3.1: Test matrix that describes the different conditions that were tested during the LOT tests.

#	MeOH [ppm]	NOx [ppm]	NO [ppm]	NO_2 [ppm]	NO/NOx [-]	CO [ppm]	O_2 [%]	H_2O [%]	CO_2 [%]	Ar [%]
1	4500	590	180	410	0.3	1220	8	5	5	balance
2	4500	590	180	410	0.3	1830	8	5	5	balance
3	4500	220	220	0	1	1220	8	5	5	balance
4	4500	710	210	500	0.3	1830	8	5	5	balance
5	2250	590	180	410	0.3	1220	8	5	5	balance

3.1.7 Concentration Scan

The second type of tests done in the SGB were concentration scan tests. The temperature and the concentration of all species, except one, were kept constant while one species' concentration varied at the time in predefined concentration levels until steady state was reached. The tests were carried out at two temperatures: T_{30} and T_{80}, which denotes the temperatures in which 30 % and 80 % conversion of methanol respectively was achieved. These two temperatures were determined through the prior LOT tests. The test matrix, which provides an overview of the concentration scans, can be seen in Table 3.2. Pre-conditioning was carried out in-between each test and a period of 30 minutes prior to each test was used to get stable flow conditions. Finally, there was a measurement period of 30 minutes in order to get representative steady-state results. The tests were carried out with the target of acquiring experimental data that could be used for model validation.

Table 3.2: Test matrix that describes the different compositions that were tested for T_{30} and T_{80} during the concentration scan test.

#	**T** [°C]	**MeOH** [ppm]	**NOx** [ppm]	**NO** [ppm]	**NO_2** [ppm]	**NO/ NOx** [-]	**CO** [ppm]	**O_2** [%]	**H_2O** [%]	**CO_2** [%]	**Ar** [%]
1/11	T_{30}/T_{80}	3000	590	180	410	0.3	1220	4	5	5	bal.
2/12	T_{30}/T_{80}	3000	590	180	410	0.3	1220	8	5	5	bal.
3/13	T_{30}/T_{80}	3000	590	180	410	0.3	1830	8	5	5	bal.
4/14	T_{30}/T_{80}	3000	590	180	410	0.3	2170	8	5	5	bal.
5/15	T_{30}/T_{80}	3000	500	0	500	0.0	1220	8	5	5	bal.
6/16	T_{30}/T_{80}	3000	220	220	0	1.0	1220	8	5	5	bal.
7/17	T_{30}/T_{80}	3000	300	90	210	0.3	1220	8	5	5	bal.
8/18	T_{30}/T_{80}	3000	710	210	500	0.3	1220	8	5	5	bal.
9/19	T_{30}/T_{80}	2250	590	180	410	0.3	1220	8	5	5	bal.
10/20	T_{30}/T_{80}	1500	590	180	410	0.3	1220	8	5	5	bal.

3.2 Modeling in GT-xCHEM

The methanol oxidation catalyst in the EATS was modeled in the software program "GT-suite" using the xCHEM add-on developed for modeling aftertreatment systems accurately. The first step in the modeling procedure was the setup of the oxidation catalyst and the flows in and out from it. Each part of the model setup was defined based on real physical data. The model was later calibrated using experimental data from the SGB testing seen in Section 3.1.

3.2.1 Methanol Oxidation Catalyst Model

The 1D model consisted of several individual parts that were all linked together, an overview of the model layout can be seen in Figure 3.4. An "Inlet" part, where flow properties such as mass flow, temperature and composition profiles were defined and the "Outlet" component was defined as a boundary with ambient conditions. The "Pipe inlet" and "Pipe outlet" represented the part of the glass tube before and after the catalyst sample.

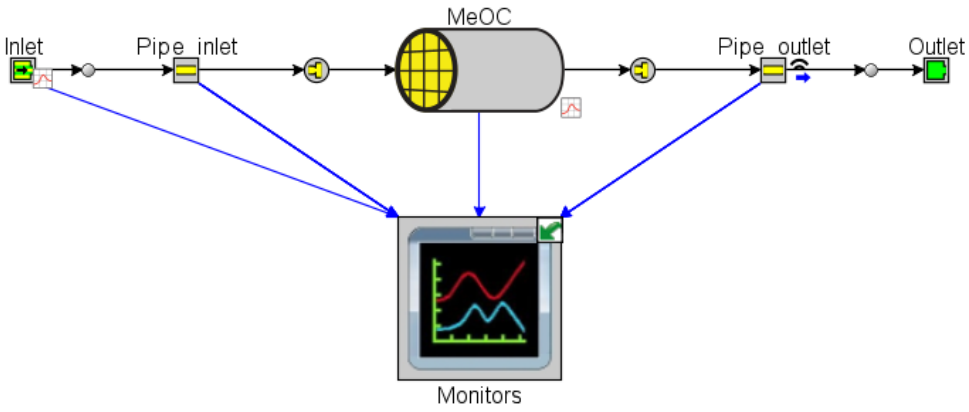

Figure 3.4: A schematic overview of the main model layout.

The MeOC was represented using the "Monolith" template available in GT-xCHEM where the catalyst properties were defined, the most important properties can be seen in Table 3.3. Thermal properties of the catalyst were also defined, these have been compiled into Table 3.4 [28]. The catalyst walls utilized a mixed diffusion model that accounted for internal mass transfer through the porous catalyst walls. A porosity of 0.5, tortuosity of 3 and mean pore size of 15 micron were the default settings in GT-xCHEM and was therefore assumed. The mixed diffusion model is based on Equation 3.1, which takes both molecular diffusion and Knudsen diffusivity, determined by Equation 3.2, into account. Where ε_{pore} is the porosity, d_{pore} is the mean pore size and τ is the tortuosity.

The monolith was assumed to be adiabatic and this has been accounted for by having a very low conductivity of the reactor walls, which can be seen in Table 3.4. This means that heat losses from the reactor to the surroundings were neglected in this study. The heat transfer between the gas and the frontal and rear face of the catalyst was modeled by neglecting heat losses from wall faces and by considering radiation losses from channel surfaces to the face openings. The flow solver employed a plug-flow reactor approach, wherein the monolith was discretized into multiple segments, and steady-state solutions were computed for each partition. Also, a fully-developed laminar flow was assumed in the monolith channels. Additionally,

the mass transfer between gas and solid phase was neglected with the argument that it was an insignificant amount compared to what is already in the gas phase.

$$\frac{1}{D_{w,j}} = \frac{\tau}{\varepsilon_{pore}} \left(\frac{1}{D_{mol,j}} + \frac{1}{D_{knud,j}} \right) \tag{3.1}$$

$$D_{knud,j} = \frac{d_{pore}}{3} \sqrt{\frac{8RT}{\pi M_j}} \tag{3.2}$$

Table 3.3: An overview of some of the most important catalyst properties defined in the "Monolith" template.

Parameter	
Frontal diameter [mm]	16
Length [mm]	16
Cell configuration [-]	Honeycomb
Channel shape [-]	Square
Cell density [1/in^2]	400
Substrate wall thickness [mm]	0.1651
Substrate thermal properties object [-]	Cordierite
Washcoat thickness [micron]	70
Washcoat thermal properties object	Alumina

Table 3.4: An overview of some of the most important thermal properties defined in the "Monolith" template.

Parameter	
Wall temperature setting [-]	Calculate wall temperature
Initial wall temperature [-]	Experiment start temperature
Number of outer wall layers [-]	2
Wall layer 1 [-]	Quartz glass
Layer 1 thickness [mm]	1
Layer 1 surface emissivity [-]	0.93
Layer 1 conductivity [(W/(m $\cdot$ K)]	3
Layer 1 density [g/cm^3]	2.2
Layer 1 specific heat [(J/(kg $\cdot$ K)]	700
Wall layer 2 [-]	Quartz wool

Parameter	
Layer 2 surface emissivity	0.93
Layer 2 conductivity [(W/(m · K)]	1E-10 (assumed adiabatic)
Layer 2 density [g/cm^3]	2.2
Layer 2 specific heat [(J/(kg · K)]	720

The reactions and mechanisms that are happening inside the catalyst were defined in the "Reactivity" template. The reactions, rate expressions and inhibition functions were defined according to Section 2.3.1.2-2.3.1.3. Table 3.5 shows some of the settings for the reactivity template.

Table 3.5: An overview of some of the most important catalyst properties defined in the "Reactivity" template.

Parameter	
Reactivity type [-]	Catalytic reactivity
Catalytic reaction rate expression basis [-]	Active material mass (mol/kg/s)
Active material loading [g/ft^3]	2
Active material dispersion parameter [-]	1
Global concentration specification [-]	mol/m^3
Aging model [-]	Disabled

To be able to analyze and compare the simulated results with experimental data, several monitors were introduced to the model. A separate subassembly object called "Monitors" was created in order to achieve structure as well as a simplified and aesthetically pleasing main view of the model components. With this, the "Monitors" component can represent a network of different monitors, which can be seen in Figure 3.5. The concentration of CO, NO, MeOH and NO_2 was monitored at both the pipe inlet and outlet. Since the concentration at the inlet was constant, the outlet concentrations were the main topic of interest. However, the inlet concentration was used to determine the conversion efficiency through a "MathEquation" object, where Equation 3.3 was computed. The calculated wall temperature of the catalyst and the inlet gas temperature were also monitored in order for them to be compared to experimental data. Lastly, a "MonitorLayout" object is used to determine the layout of the monitors.

$$\text{Conversion efficiency [\%]} = \frac{\text{Inlet concentration} - \text{Outlet concentration}}{\text{Inlet concentration}} \cdot 100\,\% \tag{3.3}$$

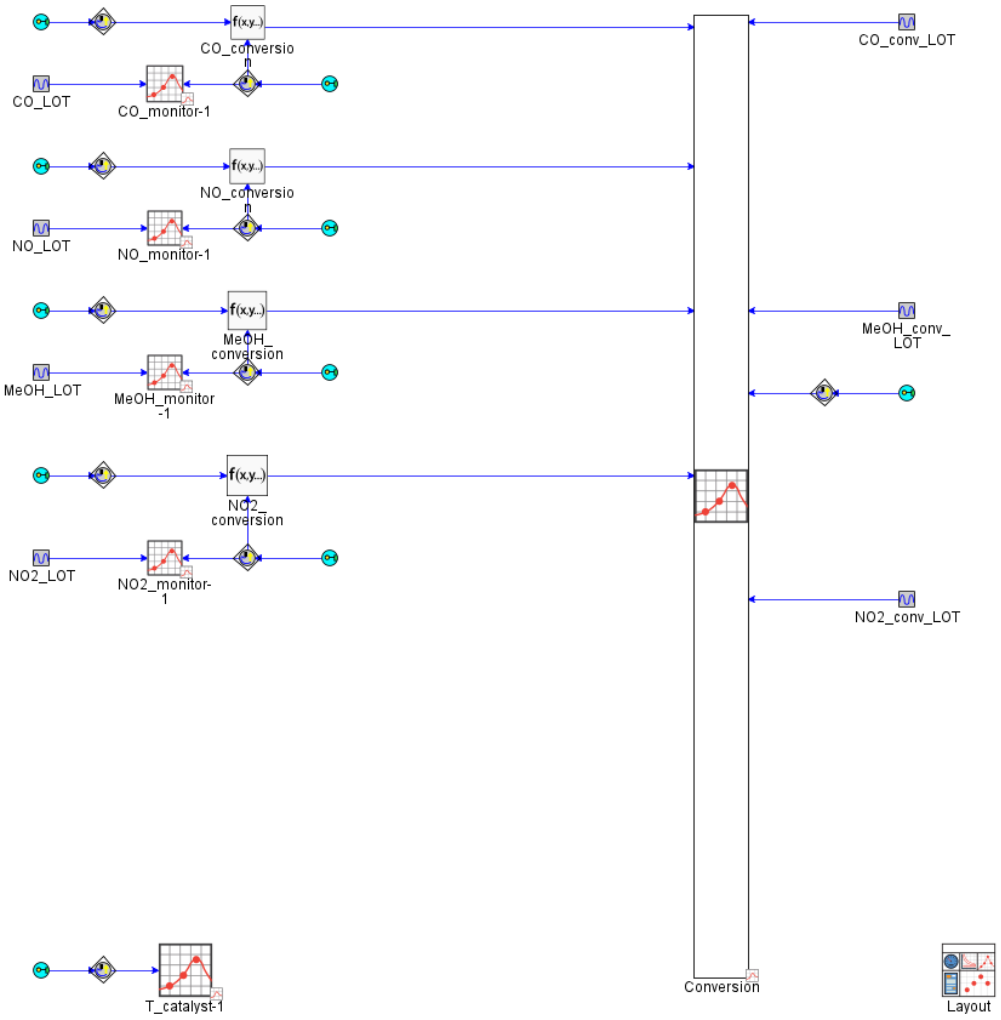

Figure 3.5: A schematic overview of the "Monitors" subassembly component.

3.2.2 Optimization and Calibration

Optimization and calibration of the kinetic parameters were done in order to fit the experimental data. This was done by altering the kinetic and inhibition parameters so that the predicted results from the model resembled the experimental data from the LOT tests as closely as possible. The first step in the calibration part was manual calibration, where the magnitude of the kinetic parameters was changed, one by one, until the trends of the predicted results and experimental results matched with acceptable accuracy. This was done for all the kinetic parameters until a range of values for each parameter was found, where the range represented a span within which the optimal solution lies, to get a good baseline before the built-in optimizer.

When the manual calibration was done and the range of the kinetic parameters was decided, the built-in optimization tool "Design optimizer" was used. This optimization tool utilized an accelerated GA as a search algorithm, where generations and population size were defined. The first optimization done with the "Design optimizer" tool was done for the methanol reactions only. This was done since the

methanol reactions were found to have the most effect on the other oxidation reactions. This optimization was done together with experimental for LOT 1-5 by utilizing the case sweep function, ensuring that all cases were satisfied to the greatest extent possible. The next step in the calibration procedure was to calibrate the inhibition parameters that affected the methanol oxidation reactions. Since the inhibition parameters affect all species, transient targeting was applied for all species. Then, the parameters for NO and NO_2 were calibrated and optimized separately concerning the inhibition parameters. All parameters, for all species, including inhibition parameters were then optimized at the same time with a wide range to match the LOT cases for all species. The final step in the optimization and calibration step was to do the entire optimization again for all parameters, with a more narrow range, which resulted in the final model.

3.2.3 Validation

The model was validated by comparing the experimental data gathered from the CS tests with predicted results from the model. Each test was configured as a separate case in the model so that the inlet composition and gas temperature could be varied. The model was then run long enough so that steady-state was reached. The predicted outlet concentrations could then be gathered from the monitors and be compared with the experimental data to evaluate the model's accuracy.

3.2.4 Scalability Test

In order to test if the model was applicable on a larger scale, a scalability test was done. The idea with the test was to see if the model prediction could be used as a tool for real aftertreatment testing. Since the catalyst used in the SGB testing was approximately 20 time smaller compared to the catalyst used in the engine tests, the specification of the catalyst needed to be modified. The catalyst length, diameter, loading and substrate wall thickness were all changed according to the full-scale catalyst specifications, which can be seen in Table 3.6. Thereafter, engine-out data used for full-scale oxidation catalyst testing, provided by Volvo Penta, was used as an input in the model. The model prediction was then compared with the steady-state system-out results obtained from the experimental testing. Three cases were evaluated where each case represented a different engine load and speed. There were some minor fluctuations in the steady-state engine-out data from the full-scale tests and the averaged data can be seen in Table 3.7 and 3.8. Please note that the highlighted value in red in Table 3.8 is a measuring error, in reality the concentration is likely close to zero.

Table 3.6: An overview of the properties of the full-scale oxidation catalyst.

Parameter	
Frontal diameter [in]	12
Length [in]	4.5

Parameter	
Active material loading [g/ft^3]	10
Cell density [1/in^2]	400
Substrate wall thickness [mm]	0.1016

Table 3.7: Summarizing table containing some average engine and exhaust data for the three different loads that were used for full-scale testing.

Load	Speed [rpm]	Torque [Nm]	T_{exh} [°C]	$\dot{m}_{exh}$ [kg/s]
1	2093	1828	423	0.795
2	1840	1386	403	0.632
3	1449	880	372	0.345

Table 3.8: An overview of the average exhaust composition before the oxidation catalyst for three different loads during full-scale testing.

Load	MeOH [ppm]	NO [ppm]	NO_2 [ppm]	CO [ppm]	O_2 [%]	H_2O [%]	CO_2 [%]	Ar [%]
1	3623	5.54	270	3800	12.0	10.5	5.80	bal.
2	5526	-0.08	206	4016	13.1	8.92	4.85	bal.
3	5819	24.0	398	3427	14.6	7.88	4.27	bal.

4

Results and Discussion

This chapter presents the results from both the SGB testing and the modeling and optimization in GT-xCHEM.

4.1 SGB Testing

Results and findings from the SGB testing will be presented in the following chapter. Key topics include the results from the LOT and CS tests and how species of interests interacted during these tests.

4.1.1 LOT Test

Comparative plots of how the injected species of interest reacted as well as general explanations and key findings from the LOT tests are presented below. The results are mainly focused on four species: MeOH, CO, NO and NO_2. Furthermore, there is a brief discussion on formaldehyde formation and its relation to MeOH oxidation.

4.1.1.1 Methanol Reactivity

Methanol was oxidized in the LOT tests, which can be seen in Figure 4.1 where the conversion of MeOH increases when the temperature is increased. All tests follow the same trend where the conversion increases rapidly after a temperature of around 220 °C, with a slight variation between tests which can be seen in Figure 4.1. This variation is probably due to the different concentrations of oxidizing agents present at each test. The conversion leveled off and reached steady-state around 85 % of conversion. The conditions at LOT 3 seem to promote MeOH oxidation since it resulted in earlier oxidation compared to the other LOT tests. On the other hand, during LOT 4 MeOH oxidized at a higher temperature compared to the other tests, although the difference between the tests are marginal.

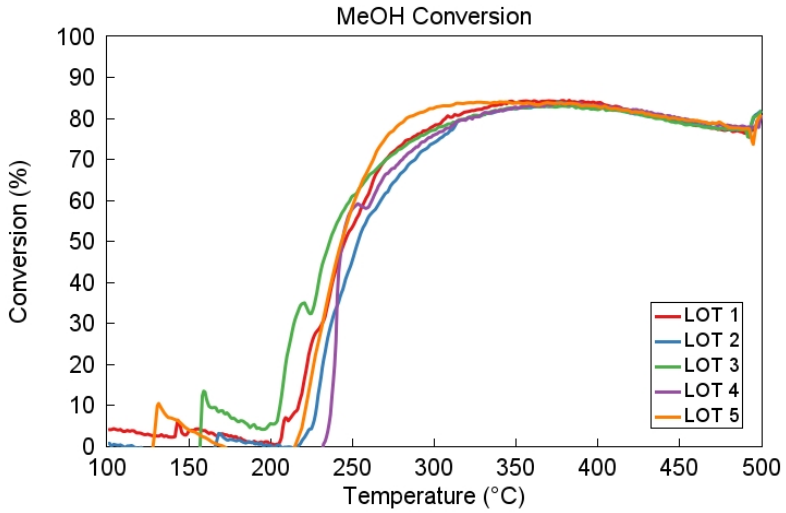

Figure 4.1: Comparative plot of methanol conversion for all performed LOT tests.

4.1.1.2 CO Reactivity

The oxidation and conversion of CO can be seen in Figure 4.2 where the five LOT tests are compared. There are some differences between the tests, even though they followed the same trend. LOT 1 and 5 are very similar, which is likely due to the same oxidizing environment in the two tests, with the only difference being the initial methanol concentration. LOT 2 and 4 are also similar, probably due to comparable environments, with only slight variations in NO_x concentration. The test that differed the most from the others was LOT 3, where no NO_2 was present. The absence of NO_2, a strong oxidizing agent, led to a delay in conversion of about 100 °C compared to the other tests. This can be explained by the fact that oxygen is the only oxidizing agent that the species compete for.

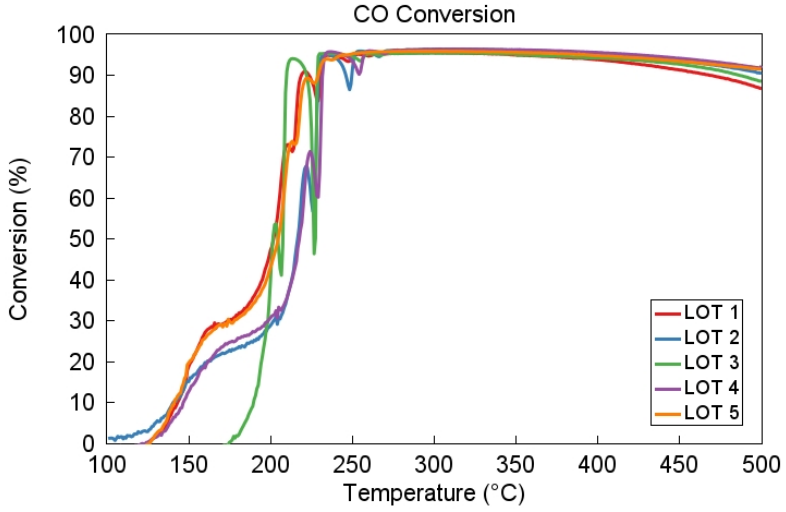

Figure 4.2: Comparative plot of CO conversion for all performed LOT tests.

4.1.1.3 NO Reactivity

NO is the primary injected species that was formed during the majority of the LOT tests, with one exception for LOT 3 where it was consumed. The outlet concentration was monitored throughout the LOT tests and can be seen in Figure 4.3. Since NO is not consumed during most of the tests a conversion plot is not presented for this species. This is because NO is formed when NO_2 is reduced, as NO_2 acts as an oxidizing agent. This phenomenon would explain why no additional NO is formed during LOT 3, since no NO_2 was injected in this test. The most probable theory is that NO is oxidized to form NO_2 in this experiment, a trend that can be seen in Figure 4.5. Additionally, it can be seen in Figure 4.3 that the concentration of NO slightly decreases at the end of each LOT. This might indicate that NO oxidation is favorable at high temperatures.

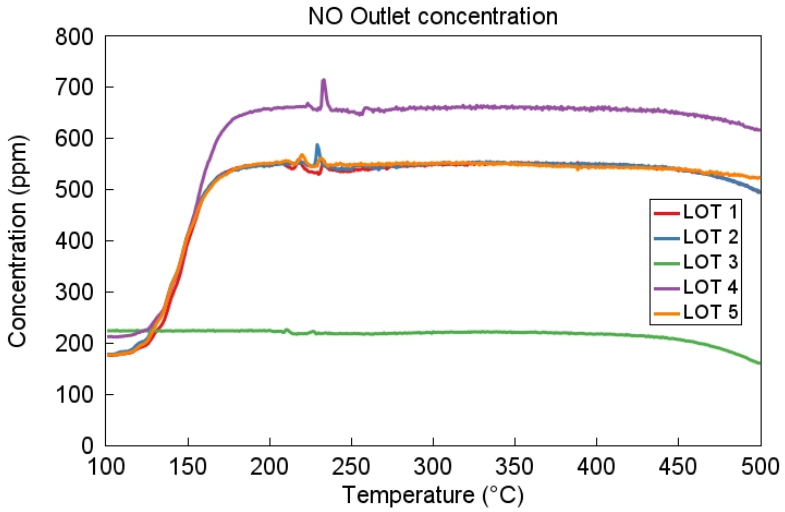

Figure 4.3: Comparative plot of the outlet concentration of NO for all performed LOT tests.

4.1.1.4 NO_2 Reactivity

It is clear that NO_2 acted as an oxidation agent in the LOT tests. The differences between the tests were minimal, which is shown in Figure 4.4. In the same figure, it can be seen that LOT 3 is not present, this is due to the absence of NO_2 in the injection. The conversion started at around 150 °C and around 90 % of the NO_2 was consumed at 200 °C. Figure 4.4 also shows that the conversion of NO_2 seem to decrease slightly at high temperatures. This could possibly be explained from Figure 4.3 that shows that the outlet concentration of NO decreases at high temperatures, potentially forming NO_2.

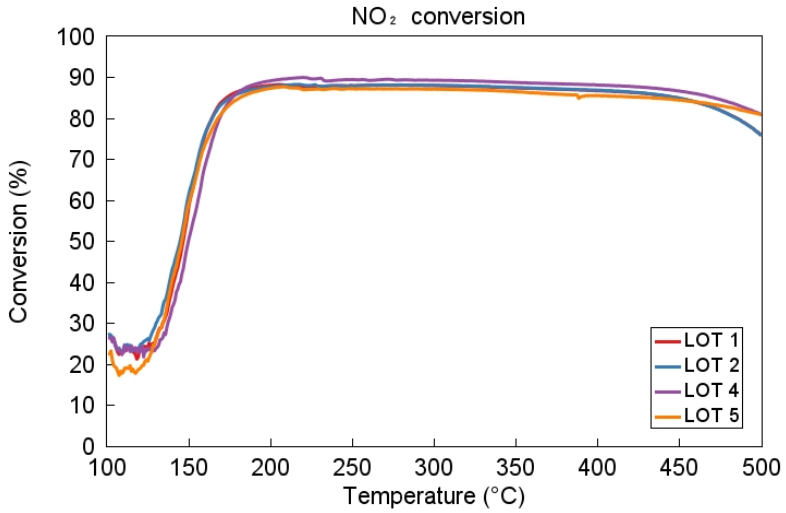

Figure 4.4: Comparative plot of NO_2 conversion for all performed LOT tests.

The outlet concentration of NO_2 was monitored throughout each LOT test, see Figure 4.5. From Figure 4.4 it can be noted that the conversion is minimal at low temperatures, due to limited reactivity. This also explains why the concentration of NO_2 is quite high at low temperatures, seen in Figure 4.5, since much of the injected NO_2 does not react. Rising temperatures promote the conversion of NO_2, which causes its outlet concentration to decrease. In LOT 3, where no initial NO_2 was injected, an interesting finding can be made, one that was mentioned in Section 4.1.1.3. It appears that no NO_2 is formed up to approximately 400°C, but afterwards some NO_2 starts to get formed, likely from NO oxidation.

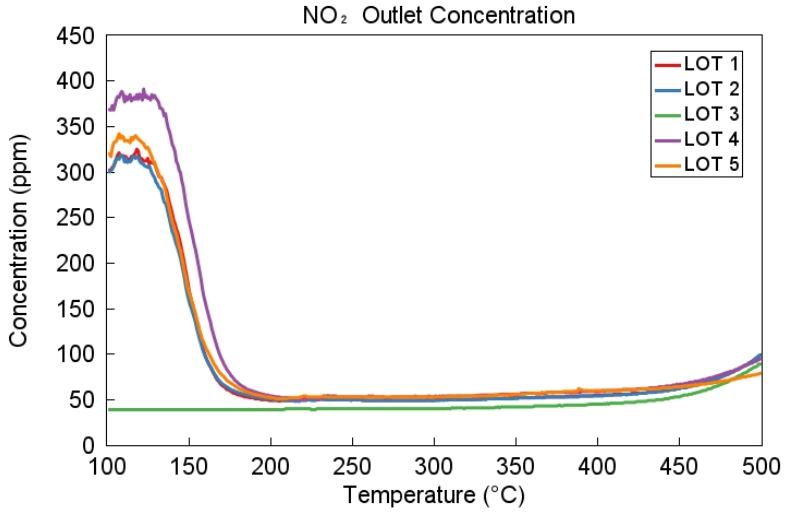

Figure 4.5: Comparative plot of NO_2 outlet concentration for all performed LOT tests.

4.1.1.5 Formaldehyde Formation

Unfortunately the measuring equipment could not be calibrated for formaldehyde due to its low boiling point and stability issues. However, it was possible to get a measuring signal of formaldehyde from the FTIR, which was later normalized to be able to illustrate its formation during the LOT tests. Figure 4.6 indicates that the formaldehyde formation decreases with lower methanol outlet concentration. The formation of formaldehyde increased at high temperatures when the methanol conversion decreased. This indicates that the formation of formaldehyde is correlated with the oxidation of methanol. The more complete oxidation of MeOH, the less formation of formaldehyde.

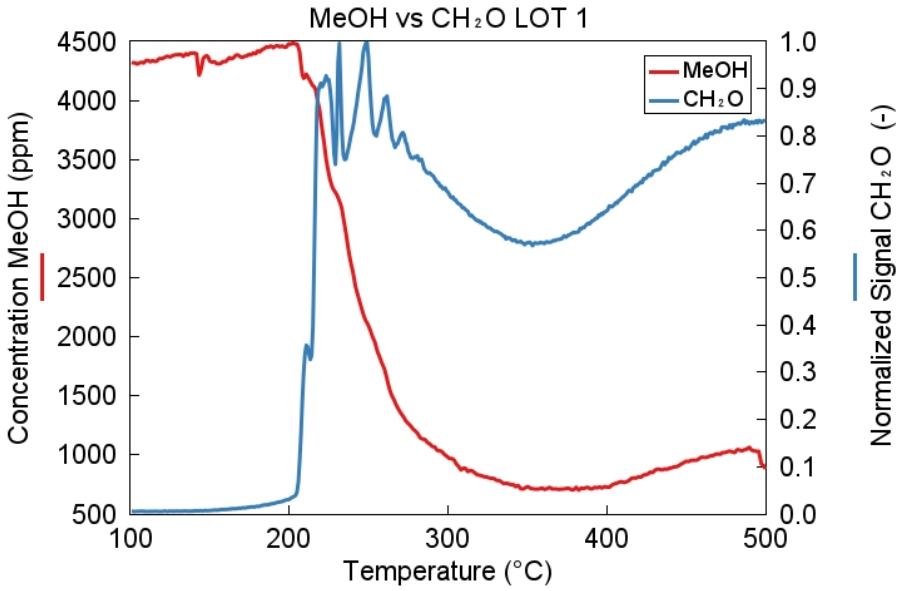

Figure 4.6: The outlet concentration of methanol and the normalized signal of CH_2O measured after the oxidation catalyst.

4.1.1.6 Conversion Temperatures of Methanol

The two different activation temperatures, T_{30} and T_{80}, were calculated for each LOT test, which can be seen in Table 4.1. The resulting average temperatures were used as constant temperature levels to perform steady-state experiments in the concentration scan tests.

Table 4.1: Temperatures at which methanol achieve 30% and 80% conversion for each LOT test and their mean value.

LOT #	T_{30} [°C]	T_{80} [°C]
1	231.8	308.3
2	237.6	321.7

LOT #	T_{30} [°C]	T_{80} [°C]
3	215.3	320.8
4	240.8	320.4
5	233.7	283.0
Mean:	**232**	**311**

4.1.2 Concentration Scan

The results from the concentration scan tests are illustrated in Table 4.2. The conversion (and formation of NO) of the species of interest have been listed, in order to see how the catalyst performs under different conditions. NO and NO_2 includes two empty cells each due to their inlet composition being zero, which means that the formation or conversion degree could not be calculated due to division by zero. One can see that the conversion of both MeOH and CO increases when the temperature is increased from 232 °C to 311 °C, since it is the corresponding conversion temperatures T_{30} and T_{80} of methanol. Additionally, if a comparison is made between test 1, where the concentration of O_2 is 4 %, and test 2 where the concentration of O_2 is 8 %, it can be seen that the conversion of MeOH and CO increases, which is reasonable since high availability of oxygen enhances oxidation.

When the concentration of CO is increased the conversion of MeOH is decreased slightly, this can be concluded when comparing tests 2 and 3. This highlights the competition for oxidizing agents between products of incomplete combustion. The lack of NO in the inlet, seen in test 5, seems to result in slightly higher MeOH and CO conversion. This could indicate that NO inhibits the oxidation of both these species. The absence of NO_2 in the inlet, as seen in test 6, does not appear to reduce the conversion of MeOH, which may seem unexpected considering that NO_2 acts as an oxidizing agent. However, the conversion of CO seems to be more affected, since its conversion is slightly lower in this test compared to test 2. The conditions at test 7 gave the highest conversion of MeOH. Therefore, having a low concentration of NO and a moderate amount of NO_2 in the exhaust gas seems to be the most favorable conditions for MeOH oxidation. The corresponding test at 311 °C, test 17, gave similar results, although test 16 had the best conversion of MeOH at 311 °C. However, it should be noted that there is a marginal outlet concentration difference of just 3 ppm between the two tests and it is unclear if the measurements are accurate enough so that a clear distinction could be made. Tests 9 and 10 both have lower inlet concentrations of MeOH, which mainly seems to result in a somewhat higher conversion of CO, probably due to the overall concentration of oxidizable species being lower.

Tests 11-20 does not need to be thoroughly discussed since they almost all seem to follow the same corresponding trends seen in tests 1-10, albeit to a lesser degree. Finally, one general trend that can be seen for all tests is that NO gets formed throughout the tests whilst NO_2 gets converted. This could be explained by that

NO_2 acts as an oxidizing agent and gets reduced to form NO.

Table 4.2: Summarizing table showing the conversion (and formation of NO) of the species of interest for all concentration scan tests.

#	T [°C]	$\mathbf{MeOH_{Conversion}}$ [%]	$\mathbf{NO_{Formation}}$ [%]	$\mathbf{NO_{2,Conversion}}$ [%]	$\mathbf{CO_{Conversion}}$ [%]
1	232	43.5	218.9	88.0	90.2
2	232	58.5	217.8	87.6	93.5
3	232	55.5	201.7	87.8	91.2
4	232	57.2	220.0	87.8	87.2
5	232	67.1	-	89.6	94.2
6	232	67.4	10.0	-	92.6
7	232	69.7	238.9	78.6	93.4
8	232	62.0	221.4	89.2	94.0
9	232	64.0	217.8	87.6	94.4
10	232	59.6	220.0	87.3	94.8
11	311	82.8	222.8	88.3	95.9
12	311	84.4	220.6	87.6	95.8
13	311	84.2	206.7	87.6	96.6
14	311	84.3	222.8	87.6	96.9
15	311	84.6	-	90.0	95.8
16	311	87.4	10.0	-	96.0
17	311	87.3	241.1	78.1	95.9
18	311	86.2	170.0	89.8	95.8
19	311	85.4	166.7	87.8	95.9
20	311	83.5	139.4	88.0	95.9

4.1.2.1 Validity of Results

Discussing the validity and reliability of the experimental measurements of the concentration scan tests is highly appropriate. This, because there were some fluctuations in the measurements for these tests which slightly affects the legitimacy and accuracy of the results. Therefore, the experimental values, seen in Table 4.2, were averaged to account for the fluctuations in the measurement signal. Figure 4.7 shows the MS measurement of the outlet concentration of MeOH for CS test 1 during the 30-minute steady-state measurement period. It can be seen that the measurements fluctuate quite a lot, somewhere in the range of ∼150 ppm, which should be taken

into consideration when comparing the results. For example, a concentration difference of 3 ppm may not be statistically significant given the overall variability, suggesting that conclusions drawn from such small differences should be approached with caution.

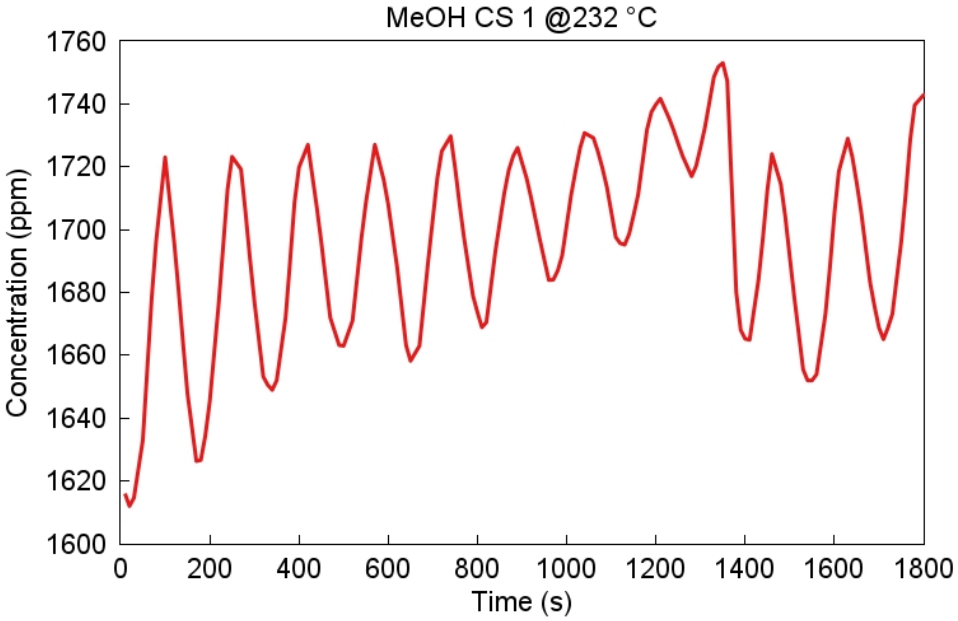

Figure 4.7: The measured outlet concentration of MeOH from CS test #1, obtained from MS.

Furthermore, it is observed that in general, the fluctuations tend to be smaller at 311 °C compared to 232 °C. Figure 4.8 shows a side-by-side comparison between the measured outlet concentration of CO for the same CS test at 232 °C and 311 °C. From the LOT test results for CO and MeOH it became apparent that there was a lot of instabilities around 232 °C, this could be why the fluctuations are more severe at this temperature compared to 311 °C. Additionally, it remains unclear if averaging the results to account for the fluctuations was representative or if another method should have been applied.

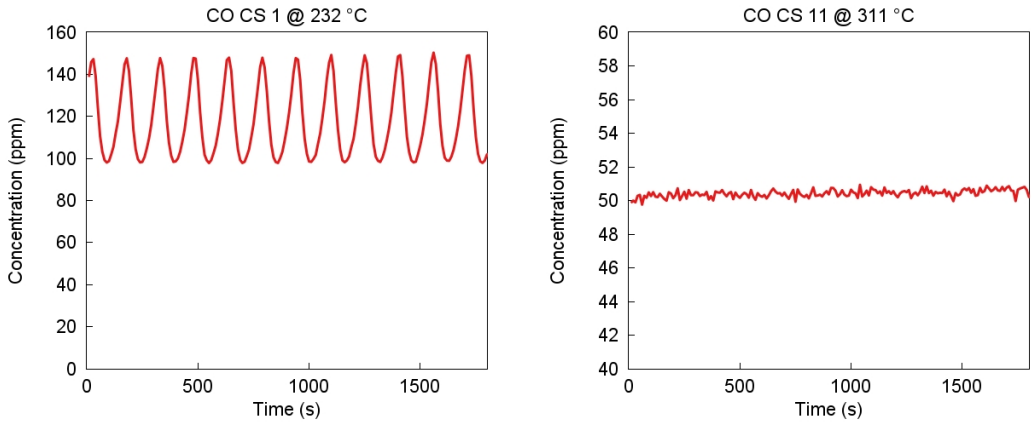

(a) Test #1 **(b)** Test #11

Figure 4.8: The measured outlet concentration of CO during CS test #1 and #11.

4.2 Modeling, Optimization and Validation

This following section consists the modeling results after the optimization, including comparisons between the experimental and predicted LOT tests, as well as validation tests between the CS tests and scalability.

4.2.1 Baseline Model

The baseline model is based on data of kinetic parameters from the literature, these are included in Appendix A.2. These values are based on a diesel oxidation catalyst (DOC) where values of methanol are based on short hydrocarbon chains (C_3H_6). These baseline values were calibrated for another catalyst with different properties and specifications which is one reason for the model performance. Figure 4.9 shows the predicted outlet concentration of the species against the measured data for LOT 1. Figure 4.9 shows that the outlet concentrations are nearly identical to the inlet concentration. This shows that there is almost no reactivity for any of the reactions, which indicates that the kinetic parameters need to be calibrated and optimized for this specific catalyst and its specifications.

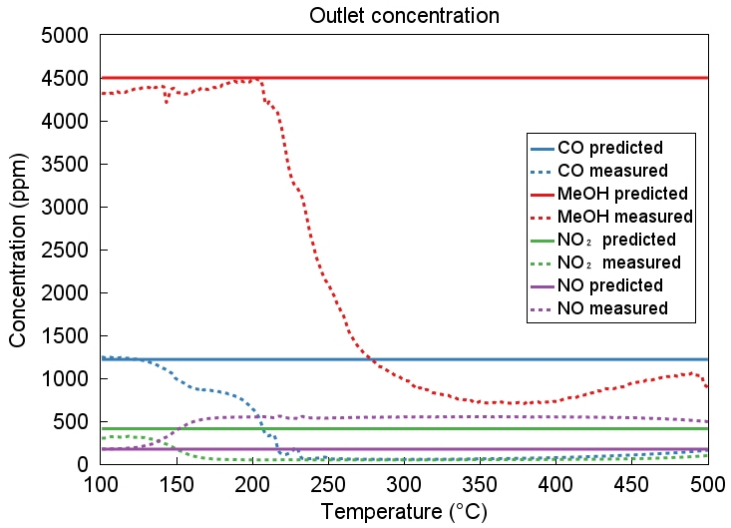

Figure 4.9: Predicted outlet concentrations using the baseline kinetic parameters compared with the measured data for LOT test 1.

4.2.2 Optimized Model

This section will present results and discussions about the final calibrated and optimized model. The predicted results will be compared with the measured data from the SGB tests. Figure 4.10 shows the conversion plot for LOT 1 where the predicted and measured results are compared, similar plots for LOT 2-5 are observable in Appendix A.1. It can be seen that the predicted results follow the same trends as the measured ones. NO is not part of the conversion plot since it is formed rather than consumed during the LOT test. The model results and accuracy of each species will be discussed later in this chapter.

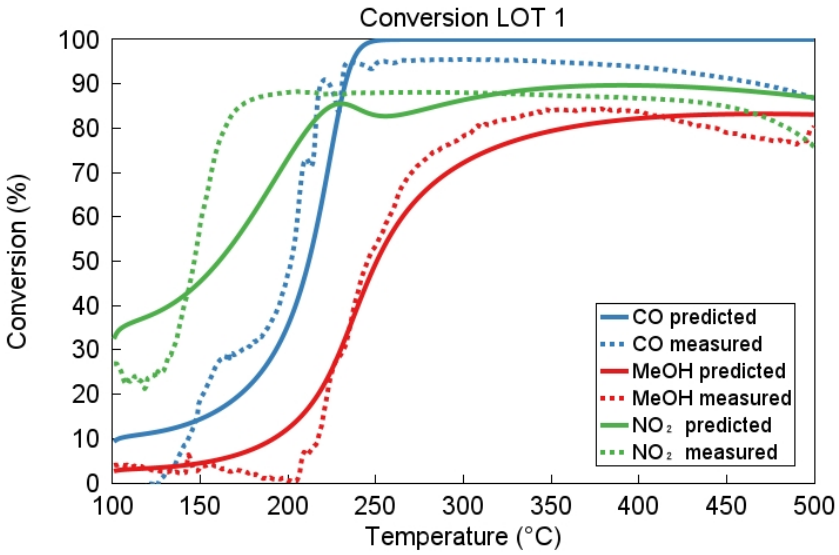

Figure 4.10: Measured and predicted conversion plot for LOT test 1.

4.2.2.1 Prediction Evaluation for CO

Figures 4.11a-4.11b shows the result for the predicted outlet concentration compared with the measured outlet concentration of CO. The only difference between LOT test 1 and 2 was that LOT test 2 had a higher inlet concentration of CO. The results indicate that the model has a relatively good predicting capability, particularly in the initial stage as well as capturing the temperature at which the catalyst becomes active for both cases. The model predicts that the outlet concentration is going down close to zero for both cases instead of stabilizing around 50 ppm as the measured results show. It can also be seen that the starting concentration of CO differ between the measured concentration and the predicted results, where the measurements indicate that the concentration level should be slightly higher than the model predicts.

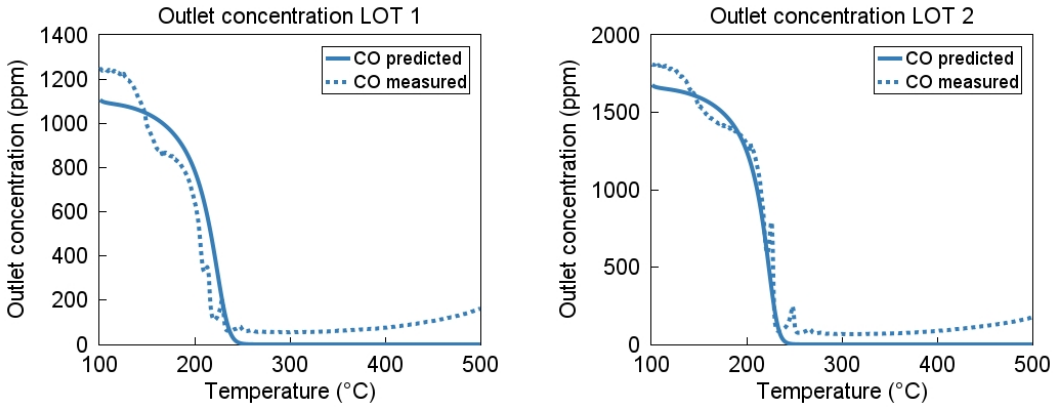

(a) LOT 1 **(b)** LOT 2

Figure 4.11: The measured and predicted outlet concentration of CO during LOT test 1 and 2.

4.2.2.2 Prediction Evaluation for MeOH

Figures 4.12a-4.12b shows the predicted outlet concentration compared to the measured outlet concentration of methanol for LOT 1 and 5. The difference between these tests is that the inlet concentration of methanol in LOT 5 was half the amount of LOT 1. The model prediction for LOT 1, illustrated in Figure 4.12a demonstrates good accuracy throughout the test. The main difference for this test is that the measurement results reveal a sharp starting point where the oxidation of methanol starts to take off, while the model prediction indicates a slower initiation of the oxidation reactions. The model prediction of LOT 5 where there is a reduced amount of methanol injected, illustrated in Figure 4.12b, points to reduced accuracy. The measurement data shows that the methanol oxidation LOT are supposed to be equivalent for both cases. However, the model presents a slower oxidation rate where less methanol is converted.

The model seems to have lower accuracy for cases where the amount of methanol is reduced which can be seen both in LOT 5 as well as in the concentration scan

comparison in Section 4.2.3 and in Table A.1. It can only be speculated why this occurs, however, one possible reason can be that the calibration and optimization are based on five different tests, four of which involve high concentration levels of methanol and only one including a lower amount. The five tests were equally weighted which means that the calibration is more influenced by cases with higher concentrations of methanol.

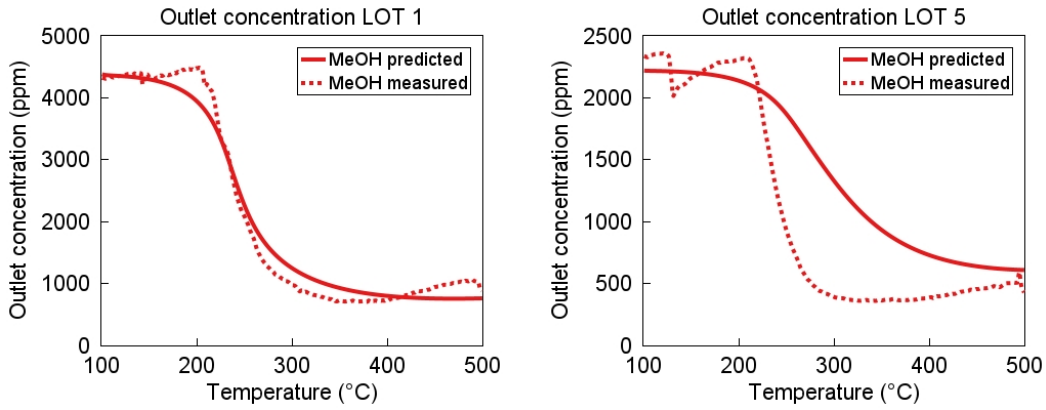

(a) LOT 1 **(b)** LOT 5

Figure 4.12: The measured and predicted outlet concentration of MeOH during LOT test 1 and 5.

4.2.2.2.1 Reaction Order Comparison

The initial approach was to use a reaction order of one for methanol which can be seen in Figure 4.13a. The model predicted a rapid oxidation where all methanol was converted as soon as the oxidation reactions started to take place. The measurement data indicated that this was not the case and therefore a reaction order of 2 for methanol was investigated. This was implemented in the final optimized model, since the model prediction was much more accurate compared to a reaction order of 1. This can be seen in Figure 4.13b.

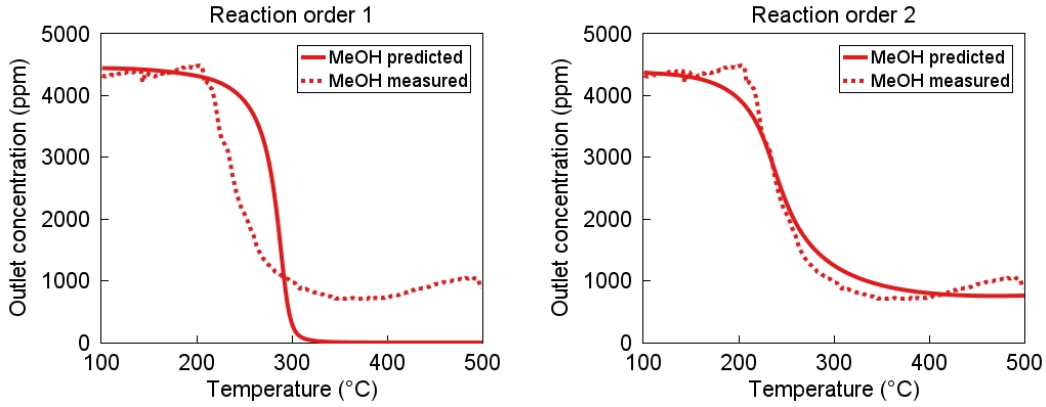

(a) Reaction order 1 **(b)** Reaction order 2

Figure 4.13: The measured and predicted outlet concentration of methanol with reaction order 1 and 2 during LOT test 1.

Methanol oxidation is less studied compared to oxidation of regular HCs, CO and NO. The reaction order for methanol oxidation is therefore more uncertain due to the limited amounts studies conducted on this particular species and subject. This incentivized the decision to investigate a reaction order of two instead, which resulted in a model with more precision. The rate expressions for methanol oxidation were adjusted accordingly, and presented in Equation 4.1 and 4.2.

$$r_{R17} = \frac{k_{R17} \left[CH_3OH\right]^2 \left[O_2\right]^{1/2}}{G} \tag{4.1}$$

$$r_{R19} = \frac{k_{R19} \left[CH_3OH\right]^2 \left[NO_2\right]}{G} \tag{4.2}$$

4.2.2.3 Prediction Evaluation for NO

Figures 4.14a-4.14b shows the predicted versus measured outlet concentrations of NO for LOT 1 and 3. The main difference between these two tests is that LOT 3 had an absence of NO_2 in the inlet. In this context, NO_2 is functioning as an oxidizing agent, facilitating the oxidation reactions of other species. As NO_2 reacts, it releases an oxygen atom and NO is formed, this can be seen in Figure 4.14a. For LOT 1, the model prediction suggests that the formation of NO is slower than what the measured data indicates. The formation seems to reach steady-state, which the model appears to predict relatively well. Figure 4.14b, representing LOT 3, shows that the model prediction is good until 400 °C where the measured data shows that NO starts to decrease. The model however is predicting a relatively constant value throughout the LOT test.

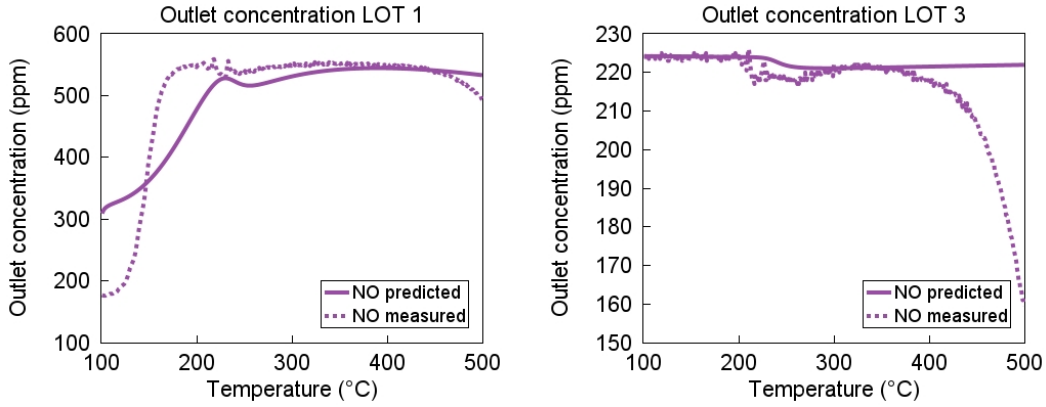

(a) LOT 1 (b) LOT 3

Figure 4.14: The measured and predicted outlet concentration of NO during LOT test 1 and 3.

4.2.2.4 Prediction Evaluation for NO_2

The predicted and measured outlet concentration of NO_2 for LOT 1 and 3 can be seen in Figure 4.15a-4.15b. The behavior of NO_2 during the LOT is closely related to the behavior of NO. When comparing Figure 4.14 and Figure 4.15 it can be concluded that the NO_2 curves are essentially inverse to the curves of NO. This could be explained by the fact that NO_2 reduces to NO as it is used as a strong oxidizing agent. This phenomenon has been thoroughly explained in multiple previous sections, so no further discussion is needed. Figure 4.15b shows that the model struggles to predict the outlet concentration of NO_2 for LOT 3, similarly to how the model struggled to predict the outlet concentration of NO for the same test. Somehow, the model would need to be configured in a way so that it recognizes the oxidation of NO to NO_2 at high temperatures. This phenomenon could unfortunately not be successfully implemented for the final optimized model.

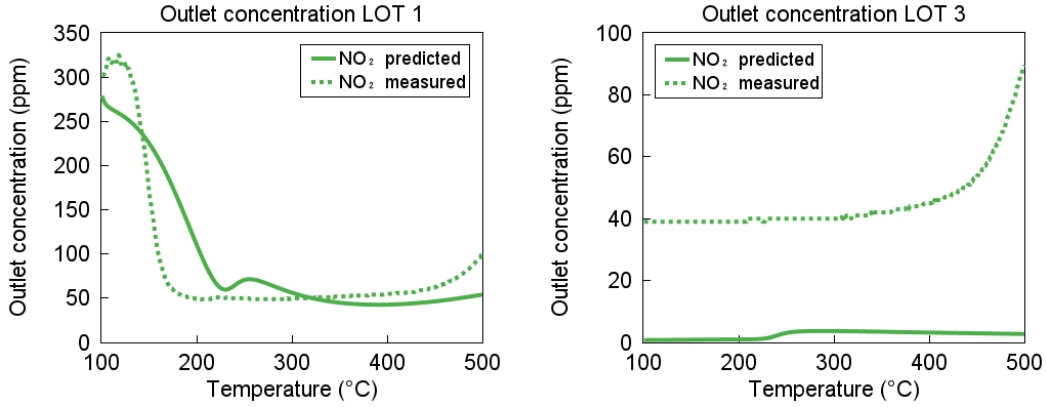

(a) LOT 1 (b) LOT 3

Figure 4.15: The measured and predicted outlet concentration of NO_2 during LOT test 1 and 3.

4.2.3 Concentration Scan Comparison

A comparison between the measured and predicted data was also done for the concentration scan tests. The measured and predicted outlet concentration of MeOH, CO, NO and NO_2 along with the absolute error can be seen in Table A.1 in Appendix A.2. Due to the overwhelming amounts of data, only some of the general trends will be discussed in this section. Therefore, a more concise version of the table has been constructed, including average, median, maximum and minimum absolute error for each specie at T_{30} and T_{80}, see Table 4.3. The model is best at predicting MeOH concentrations at 232 °C and when the inlet concentration is 3000 ppm, the absolute error for these cases is in the range of 2.2-25.4 %. For CS tests 9 and 10 where the inlet concentration of MeOH is decreased to 2250 and 1500 ppm, the error goes up to 45.0 and 62.7 % respectively. Further, the model is worse at predicting the outlet concentration when the temperature is increased to 311 °C. For CS tests 11-20 the average absolute error is 87.6 %.

One can also see, when looking at Table 4.3, that the absolute error between the predicted and measured CO concentrations are in the range of 99.7 to 100 %. This can be explained by the fact that the predicted outlet concentration is very close to zero, meaning that according to the model CO is essentially fully oxidized. However, the measured data from the experiments says otherwise and in reality the conversion of CO never reached 100 %.

Additionally, it can be seen in Table 4.3 that the model is particularly good at predicting the concentration of NO, where absolute error lies in a range from as low as 1.3 % to 24.8 % at its peak, with most cases having an average error of 8.3 and 9.5 % at T_{30} and T_{80} respectively. The maximum error happens for CS test 20 in which the concentration of MeOH is 1500 ppm (half of the baseline value of 3000 ppm). However, this test resulted in a high absolute error for all species, not only NO, which indicates that the model is better optimized for higher concentrations of MeOH.

Lastly, it was identified that the model prediction of NO_2 concentration was worse at 232 °C compared to 311 °C. At the lower temperatures the mean absolute error was 35.8 % compared to 25.3 % at 311 °C. The model predicted the concentration well at all tests except two at 311 °C, which were CS tests 16 and 17. The common factor for these two tests seems to be that the inlet concentration of NO_2 is 0 and 210 ppm, which is much lower compared to the other cases.

Table 4.3: Average, median, maximum and minimum absolute errors for each species during the CS tests at T_{30} and T_{80}.

Species	**T [°C]**	**Average error [%]**	**Median error [%]**	**Maximum error [%]**	**Minimum error [%]**
MeOH	T_{30}	21.5	14.4	62.7	2.2
	T_{80}	87.6	71.9	166.0	58.0

Species	T [°C]	Average error [%]	Median error [%]	Maximum error [%]	Minimum error [%]
CO	T_{30}	100.0	100.0	100.0	99.7
	T_{80}	100.0	100.0	100.0	100.0
NO	T_{30}	8.3	8.2	11.1	2.0
	T_{80}	9.5	6.9	24.8	1.3
NO_2	T_{30}	35.8	35.1	90.0	6.0
	T_{80}	25.3	14.1	92.9	2.0

4.2.4 Scalability

The predicted and measured conversions were monitored and compared at each of the three operating points throughout the engine test. Figure 4.16 shows the comparison between the predicted and measured conversion for Load 1. Similar results and figures for Load 2 and Load 3 are presented in Appendix A.3. It can be seen that the conversion of CO reaches 100 %, a reoccurring phenomenon that have been discussed in previous sections and can be considered one of the main weaknesses with the model. The model predicts the conversion of both MeOH and NO_2 very well, especially considering that the catalysts are vastly different from each other regarding both the loading and dimensions. Since NO was mostly formed rather than consumed in the oxidation catalyst it is not included in Figure 4.16. Instead, the predicted and measured outlet concentration of NO during Load 1 of the scalability test can be seen in Figure 4.17. The figure shows how the predicted concentration follows the measured concentration well. However, the predicted concentration is slightly lower compared to the measured concentration.

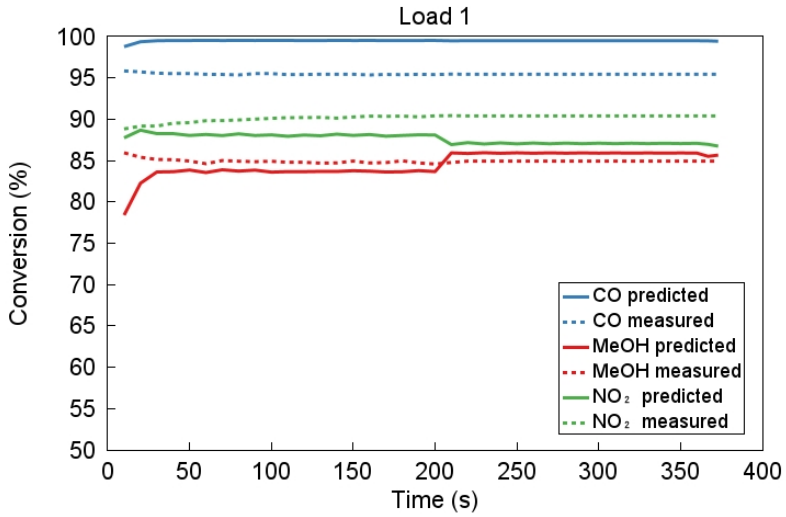

Figure 4.16: Comparing plot of the predicted and measured conversion throughout the engine test for load 1 of the scalability test.

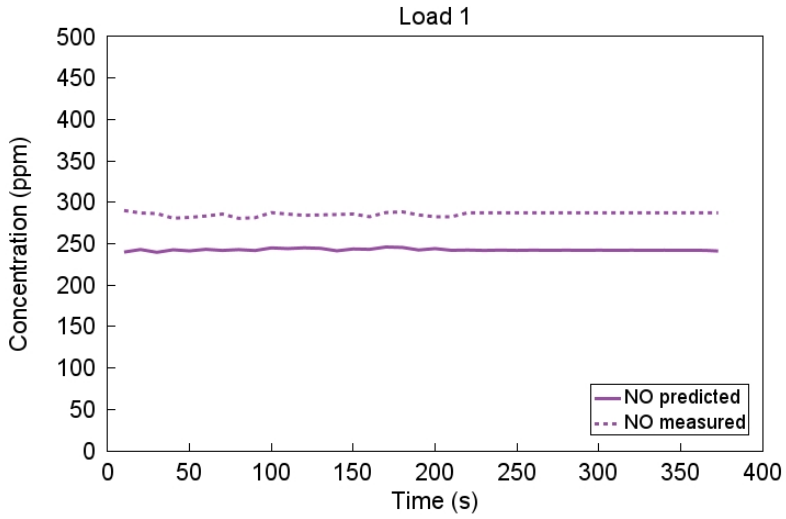

Figure 4.17: Comparing plot of the predicted and measured outlet concentration of NO throughout the engine test for load 1 of the scalability test.

4.2.4.1 Sources of Errors

The scalability test had some sources of errors that are worth discussing. The test was conducted and simulated using the original model, with only minor modifications. While the catalyst properties and inlet flow were adjusted to align with the real test environment, no thermal adjustments were made which probably had some impact on the result. Since chemical reactions are temperature dependent, a more accurate setup of the thermal profile similar with the actual testing scenario could increase the accuracy of the predicted values.

Another factor to consider is the reactions used in the model. The real testing was conducted on a dual-fuel system, which means that diesel and methanol were blended. However, the reactions within the model are the same as for the original case, neglecting other reactions such as diesel- and formaldehyde oxidation. Including these reactions in the model could significantly influence the result, as some of the reactions are exothermic and release heat. Furthermore, it is important to note that the species involved in the test influence each other through inhibition which may impact the overall results.

5

Conclusion and Future Work

This final chapter concludes and summarizes the findings of the master's thesis as well as presents recommendations for future work and studies.

5.1 Conclusion

Several conclusions could be drawn from the results of this thesis and most of the topics of uncertainty could either be answered or clarified.

The results indicate that it is indeed possible to model a Methanol Oxidation Catalyst successfully in GT-xCHEM with experimental data gathered from SGB testing. Distinct reactivity patterns under varying conditions could be seen for all species of interest: MeOH, CO, NO and NO_2. The final optimized model proved to correlate well with experimental data, particularly for species MeOH, NO and NO_2, suggesting that modeling could be a useful tool for predicting catalyst performance and complement physical testing.

It can be concluded that there exists interdependent interactions between the species, particularly related to oxidizing agents and inhibition. For example, the absence of NO_2 in certain tests led to CO converting at a higher temperature than usual, which emphasizes the role of oxidizing agents and availability of them. Additionally, competition for oxidizing agents also had a substantial impact on the individual conversion rates of each species. The struggle of predicting the formation of NO and NO_2 further illustrates the complexity of modeling chemical reactions. Formaldehyde could unfortunately not be monitored in detail but its formation was found to be highly dependent on incomplete oxidation of MeOH.

The performance of the oxidation catalyst varied depending on different operating conditions, this was demonstrated in both the LOT tests and in the concentration scan tests. From the LOT tests it was revealed that MeOH strongly oxidized at temperatures above 220 °C, achieving a maximum conversion of approximately 85 %. The presence of NO_2 was identified as a key parameter for enhancing the oxidation rates of CO and MeOH. Additionally, optimizing operating conditions to favor complete oxidation of MeOH is of great significance to minimize formaldehyde emissions.

Lastly, scaling up the model to simulate a full-sized dual-fuel methanol-diesel, or 100 % methanol, engines appears feasible. The successful predictions of conversion

rate at different loads during the scalability test strongly supports this belief. In particular, the model's ability to predict the behavior of MeOH, NO and NO_2, despite the differences in catalyst properties and other sources of error, further supports the potential for larger scale applications. However, the model's limitations in predicting CO conversion, which fully oxidized in the simulations, highlight the need for further refinement before the model can be used to accurately represent real-world conditions.

5.2 Future Work

After conducting the thesis a few key points regarding recommendations for future work in this field were identified. These have been briefly discussed and summarized below:

- **Run fewer concentration scan tests at more temperature levels:** Initially the thought was that the concentration scan tests could be used to calibrate the kinetic and inhibition parameters. However, it turned out that the LOT tests were more useful in this regard and the concentration scan tests ended up mainly being used for validation and accuracy evaluation. A recommendation would be to run fewer test at more temperature levels to get more steady-state data points which could be used to determine kinetic parameters better.
- **Isolate reactions during testing:** Isolating reactions more instead of performing SGB testing with full mixtures of all species might be helpful to determine kinetic and inhibition parameters for reactions individually.
- **Investigate inhibition more extensively:** Inhibition seems to be a quite complex topic that has a relatively large impact on the governing reactions in the oxidation catalyst. Investigating inhibition more extensively, both using literature and testing, might result in a more accurate model.
- **Investigate reaction order of MeOH:** The reaction order of MeOH had a large impact on how the model predicted its conversion. Therefore, doing additional testing to study the reaction order is advisable to confirm that the model complies with reality well.
- **Improve model prediction of CO conversion:** The main limitation with the final optimized model was that the model predicted that CO was fully oxidized as soon as the temperature was sufficiently high. In reality, and according to the SGB testing, the conversion reached a maximum point and stabilized after a certain temperature, a phenomena which the model could not successfully predict. Exactly how to account for this behavior is unclear and due to this it is considered a topic for future work and studies.
- **Improve model prediction of high temperature NO oxidation:** High temperature oxidation of NO was seen during the LOT tests. However, the model struggled to account for this phenomenon, this was especially prominent

for LOT 3 where no NO_2 was introduced in the inlet. This can be considered a minor flaw in the model which needs further work.

- **Implement formaldehyde in the model:** Since the concentration of formaldehyde could not be measured with the measuring equipment in the laboratory due to stability issues, it was not possible to implement formaldehyde reactions to the model. Formaldehyde is a problematic emission gas which needs to be minimized in order for MeOH engines to be feasible. Also, it could potentially increase the overall model prediction accuracy since the SGB data included formaldehyde formation, which could not be accounted for in the current model. Due to this, finding a way to measure formaldehyde concentration and implement it is crucial to predict and model methanol oxidation catalysts.
- **More extensive data management:** The raw data from the SGB testing was implemented directly to optimize the model without any pre-treatment or management due to time limitations. Measuring errors and outliers are normal when doing tests and could have affected the model. Therefore, removing suspected outliers and nonphysical behavior could make the model predictions more accurate.
- **Apply the same methodology for a full-scale oxidation catalyst:** Due to resource and complexity limitations, the SGB testing was performed on laboratory scale. It would be interesting to apply the same methodology to a pilot-scale, or even full-scale, oxidation catalyst to investigate if an even more accurate model can be created.

Bibliography

[1] C. S. Sampara, E. J. Bissett, and M. Chmielewski, "Global kinetics for a commercial diesel oxidation catalyst with two exhaust hydrocarbons," *Industrial & Engineering Chemistry Research*, vol. 47, no. 2, pp. 311–322, 2008. [Online]. Available: https://doi.org/10.1021/ie070813x

[2] S. Herceg, N. Vladimir, L. Boban, and V. Soldo, "Overview of technical and operational measures for emission reduction in the marine sector," in *2021 6th International Conference on Smart and Sustainable Technologies (SpliTech)*, 2021, pp. 1–6.

[3] European Environment Agency and European Maritime Safety Agency, "Facts and figures: The emter report," Copenhagen, Denmark and Lisbon, Portugal, 2021, reproduction is authorised provided the source is acknowledged. [Online]. Available: https://www.emsa.europa.eu/about/financial-regulations/items.html?cid=14&id=4515

[4] C. Yao, C.S. Cheung, C. Cheng, Y. Wang, T.L. Chan, and S.C. Lee, "Effect of diesel/methanol compound combustion on diesel engine combustion and emissions," *Energy Conversion and Management*, vol. 49, no. 6, pp. 1696–1704, 2008. [Online]. Available: https://www.sciencedirect.com/science/article/pii/S0196890407004104

[5] M. Jiang, W. Sun, L. Guo, H. Zhang, Z. Jia, Z. Qin, G. Zhu, C. Yu, and J. Zhang, "Numerical optimization of injector hole arrangement for marine methanol/diesel direct dual fuel stratification engines," *Applied Thermal Engineering*, vol. 257, p. 124456, 2024. [Online]. Available: https://www.sciencedirect.com/science/article/pii/S1359431124021240

[6] International Renewable Energy Agency (IRENA), "Innovation outlook: Renewable methanol," https://www.irena.org/-/media/Files/IRENA/Agency/Publication/2021/Jan/IRENA_Innovation_Renewable_Methanol_2021.pdf, 2021, accessed: 2025-01-29.

[7] Femto Engineering, "1D System Simulation," 2019, accessed: 2025-01-24. [Online]. Available: https://www.femto.eu/stories/1d-system-simulation/

[8] P. Li, A.-T. Nguyen, H. Du, Y. Wang, and H. Zhang, "Polytopic LPV approaches for intelligent automotive systems: State of the art and future challenges," *Mechanical Systems and Signal Processing*, vol. 161, p. 107931,

2021. [Online]. Available: https://www.sciencedirect.com/science/article/pii/S0888327021003265

[9] Z. Lv, G. He, W. Zhang, J. Liu, Z. Lian, Y. Yang, Z. Yan, G. Xu, W. Shan, Y. Yu, and H. He, "Interface sites on vanadia-based catalysts are highly active for NOx removal under realistic conditions," *Journal of Environmental Sciences*, vol. 136, pp. 523–536, 2024. [Online]. Available: https://www.sciencedirect.com/science/article/pii/S100107422200496X

[10] A. W. Majewski, "Selective catalytic reduction," *DieselNet*, 2023. [Online]. Available: https://dieselnet.com/tech/cat_scr.php

[11] A. Russell and W. S. Epling, "Diesel oxidation catalysts," *Catalysis Reviews*, vol. 53, no. 4, pp. 337–423, 2011.

[12] A. Winkler, D. Ferri, and M. Aguirre, "The influence of chemical and thermal aging on the catalytic activity of a monolithic diesel oxidation catalyst," *Applied Catalysis B: Environmental*, vol. 93, no. 1, pp. 177–184, 2009. [Online]. Available: https://www.sciencedirect.com/science/article/pii/S0926337309003816

[13] F. Huang, D. Huang, M. Wan, J. Lei, and L. Shen, "Experimental investigation on effects of diesel oxidation catalysts on emission characteristics of a methanol-diesel dual-fuel engine," *Journal of Energy Engineering*, vol. 151, no. 1, p. 04024040, 2025. [Online]. Available: https://ascelibrary.org/doi/abs/10.1061/JLEED9.EYENG-5804

[14] D. Chen, T. Wang, T. Yang, G. Li, Y. Chen, and T. Qiao, "Effects of egr combined with doc on emission characteristics of a two-stage injected fischer-tropsch diesel/methanol dual-fuel engine," *Fuel*, vol. 329, p. 125451, 2022. [Online]. Available: https://www.sciencedirect.com/science/article/pii/S0016236122022840

[15] B. A. Zincir and Y. Arslanoglu, "Comparative life cycle assessment of alternative marine fuels," *Fuel*, vol. 358, p. 129995, 2024. [Online]. Available: https://www.sciencedirect.com/science/article/pii/S0016236123026091

[16] C. Mohd Noor, M. Noor, and R. Mamat, "Biodiesel as alternative fuel for marine diesel engine applications: A review," *Renewable and Sustainable Energy Reviews*, vol. 94, pp. 127–142, 2018. [Online]. Available: https://www.sciencedirect.com/science/article/pii/S1364032118303770

[17] U.S. Energy Information Administration, "Biodiesel basics," https://www.eia.gov/energyexplained/biofuels/biodiesel-rd-other-basics.php, 2025, accessed: 2025-01-28.

[18] A. T. Khadim, T. M. Albayati, and N. M. Cata Saady, "Removal of sulfur compounds from real diesel fuel employing the encapsulated mesoporous material adsorbent co/mcm-41 in a fixed-bed column," *Microporous and Mesoporous Materials*, vol. 341, p. 112020, 2022. [Online]. Available: https://www.sciencedirect.com/science/article/pii/S1387181122003389

[19] N. Wissner, S. Healy, D. M. Cames, and J. Sutter, "Methanol as a marine fuel," Öko-Institut e.V., Tech. Rep., 2023, accessed: 2025-01-29. [Online]. Available: https://www.oeko.de/fileadmin/oekodoc/Methanol-as-a-marine-fuel.pdf

[20] B. Zincir and C. Deniz, *Methanol as a Fuel for Marine Diesel Engines*. Singapore: Springer Singapore, 2021, pp. 45–85. [Online]. Available: https://doi.org/10.1007/978-981-16-0931-2_4

[21] American Petroleum Institute, "Ultra-low sulfur diesel (ulsd) issue paper," n.d., accessed: 2025-05-13. [Online]. Available: https://www.api.org/-/media/Files/Policy/Fuels-and-Renewables/US-Fuel-Requirements/ULSD-Issue-Paper.pdf

[22] C. Depcik and D. Assanis, "One-dimensional automotive catalyst modeling," *Progress in Energy and Combustion Science*, vol. 31, no. 4, pp. 308–369, 2005. [Online]. Available: https://www.sciencedirect.com/science/article/pii/S0360128505000237

[23] R. A. van Santen, *Modern Heterogeneous Catalysis: An Introduction*. Newark: John Wiley & Sons, Incorporated, 2017.

[24] J. Zheng, Z. M. Png, S. H. Ng, G. X. Tham, E. Ye, S. S. Goh, X. J. Loh, and Z. Li, "Vitrimers: Current research trends and their emerging applications," *Materials Today*, vol. 51, pp. 586–625, 2021. [Online]. Available: https://www.sciencedirect.com/science/article/pii/S1369702121002261

[25] T. J. Wang, S. W. Baek, and J.-H. Lee, "Kinetic parameter estimation of a diesel oxidation catalyst under actual vehicle operating conditions," *Industrial & Engineering Chemistry Research*, vol. 47, no. 8, pp. 2528–2537, 2008. [Online]. Available: https://doi.org/10.1021/ie071306i

[26] A. V. Karre, R. K. Garlapalli, A. Jena, and N. Tripathi, "State of the art developments in oxidation performance and deactivation of diesel oxidation catalyst (doc)," *Catalysis Communications*, vol. 179, p. 106682, 2023. [Online]. Available: https://www.sciencedirect.com/science/article/pii/S1566736723000845

[27] D. E. Goldberg, *Genetic Algorithms in Search, Optimization, and Machine Learning*, 1st ed. Boston, MA, USA: Addison-Wesley Longman Publishing Co., Inc., 1989.

[28] Engineering Toolbox, "Emissivity coefficients," n.d., accessed: 2025-03-25. [Online]. Available: https://www.engineeringtoolbox.com/emissivity-coefficients-d_447.html

A

Appendix 1

A.1 Light-Off Temperature Test

Figure A.1-A.5 shows the predicted and measured conversion and outlet concentration of species of interest for all the light-off temperature tests.

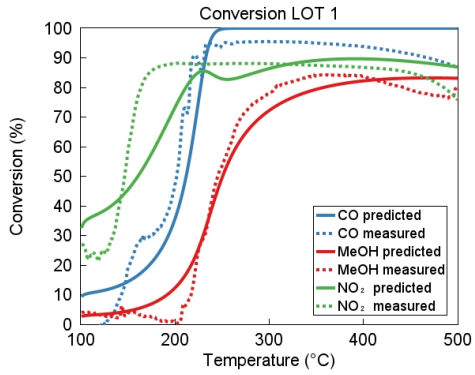

(a) Conversion

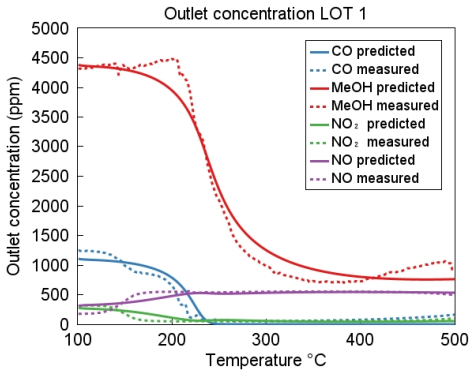

(b) Outlet concentration

Figure A.1: The measured and predicted conversion and outlet concentration for LOT test 1.

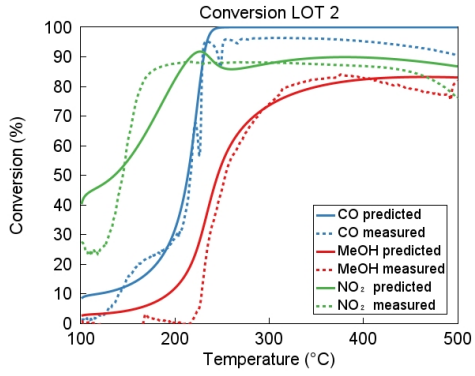

(a) Conversion

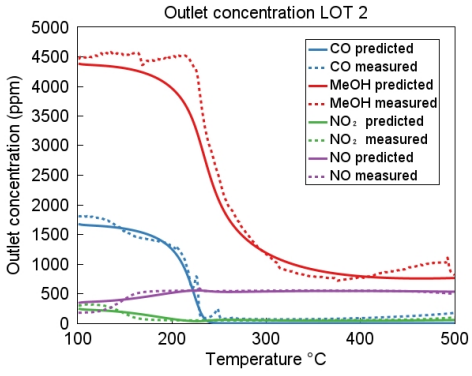

(b) Outlet concentration

Figure A.2: The measured and predicted conversion and outlet concentration for LOT test 2.

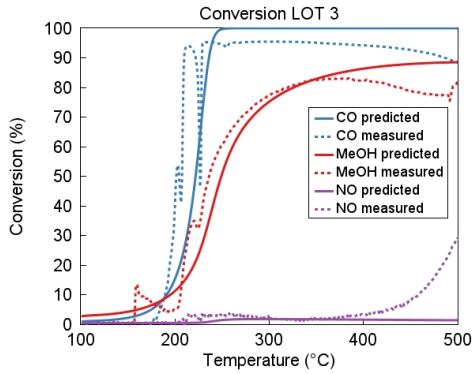

(a) Conversion

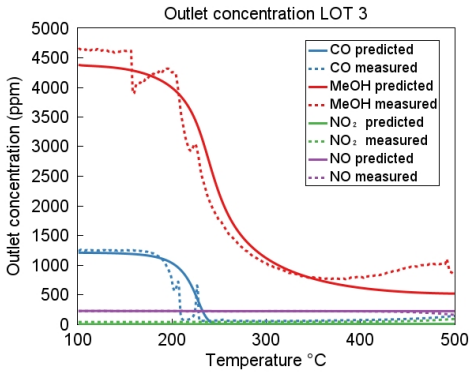

(b) Outlet concentration

Figure A.3: The measured and predicted conversion and outlet concentration for LOT test 3.

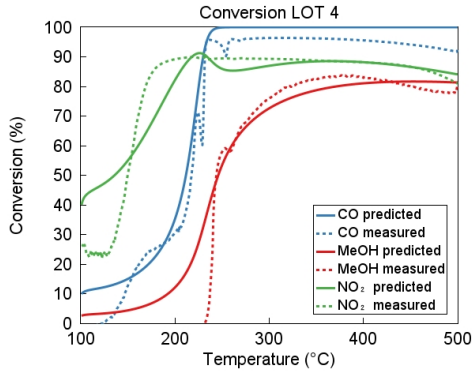

(a) Conversion

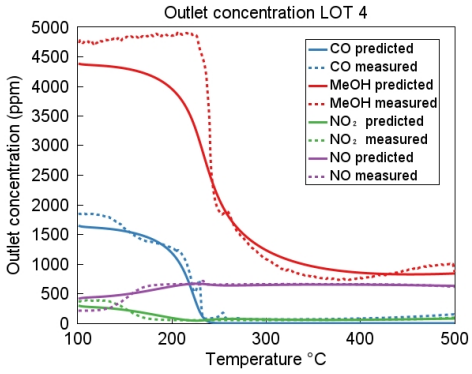

(b) Outlet concentration

Figure A.4: The measured and predicted conversion and outlet concentration for LOT test 4.

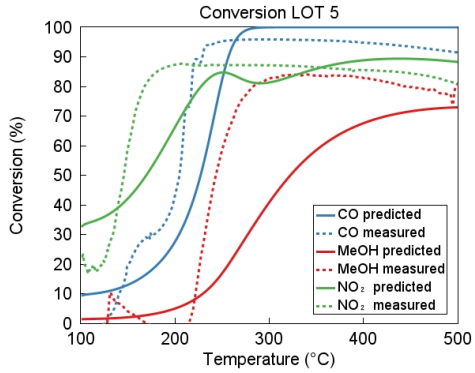

(a) Conversion

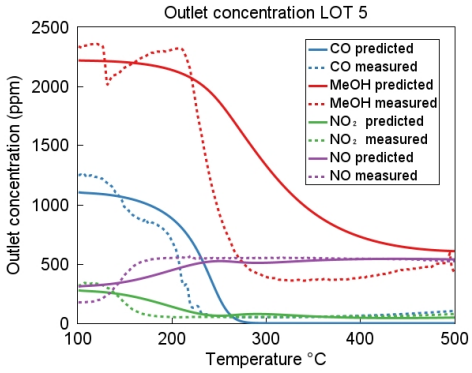

(b) Outlet concentration

Figure A.5: The measured and predicted conversion and outlet concentration for LOT test 5.

A.2 Concentration Scan Comparison

The measured outlet concentrations from the concentration scan tests compared with the predicted concentrations from the GT-xCHEM model can be seen in Table A.1. The absolute error was calculated by taking the difference between the measured and predicted concentration divided by the measured concentration. A more detailed discussion of the table could be seen in Section 4.2.3.

Table A.1: A comparative table that presents the measured and predicted outlet concentrations of the investigated species during the concentration scan tests.

Species	**T [°C]**	**#**	**Measured concentration [ppm]**	**Predicted concentration [ppm]**	**Absolute error [%]**
MeOH	232	1	1695	1527	9.9
		2	1246	1218	2.2
		3	1334	1158	13.2
		4	1284	1127	12.2
		5	987	1185	20.1
		6	978	1130	15.5
		7	910	1141	25.4
		8	1141	1245	9.1
		9	811	1176	45.0
		10	606	986	62.7
	311	11	515	996	93.4
		12	468	780	66.7
		13	473	766	61.9
		14	470	759	61.5
		15	462	730	58.0
		16	379	644	69.9
		17	382	664	73.8
		18	413	821	98.8
		19	329	743	125.8
		20	247	657	166.0

Species	T [°C]	#	Measured concentration [ppm]	Predicted concentration [ppm]	Absolute error [%]
CO	232	1	119	0.0613	99.9
		2	79	0.0132	100.0
		3	161	0.0115	100.0
		4	277	0.0103	100.0
		5	70	0.0111	100.0
		6	90	0.0096	100.0
		7	80	0.0097	100.0
		8	73	0.0147	100.0
		9	68	0.0533	99.9
		10	64	0.1938	99.7
	311	11	50	4.58E-4	100.0
		12	51	2.93E-4	100.0
		13	62	3.74E-4	100.0
		14	67	4.06E-4	100.0
		15	51	2.68E-4	100.0
		16	49	2.29E-4	100.0
		17	50	2.37E-4	100.0
		18	51	3.17E-4	100.0
		19	50	4.61E-4	100.0
		20	50	7.49E-4	100.0
NO	232	1	574	529	7.8
		2	572	524	8.4
		3	543	532	2.0
		4	576	535	7.1
		5	466	429	7.9
		6	242	216	10.7
		7	305	271	11.1
		8	675	629	6.8
		9	572	517	9.6
		10	576	512	11.1

Species	T [°C]	#	Measured concentration [ppm]	Predicted concentration [ppm]	Absolute error [%]
	311	11	581	546	6.0
		12	577	543	5.9
		13	552	545	1.3
		14	581	546	6.0
		15	429	456	6.3
		16	242	217	10.3
		17	307	284	7.5
		18	567	649	14.5
		19	480	541	12.7
		20	431	538	24.8
NO_2	232	1	49	58	18.4
		2	51	64	25.5
		3	50	56	12.0
		4	50	53	6.0
		5	52	70	34.6
		6	40	4	90.0
		7	45	29	35.6
		8	54	81	50.0
		9	51	71	39.2
		10	52	76	46.2
	311	11	48	42	12.5
		12	51	45	11.8
		13	51	43	15.7
		14	51	42	17.6
		15	50	44	12.0
		16	42	3	92.9
		17	46	16	65.2
		18	51	60	17.6
		19	50	47	6.0
		20	49	50	2.0

A.3 Scalability Test

Figure A.6-A.8 shows the predicted and measured conversion and outlet concentration for each engine load and speed.

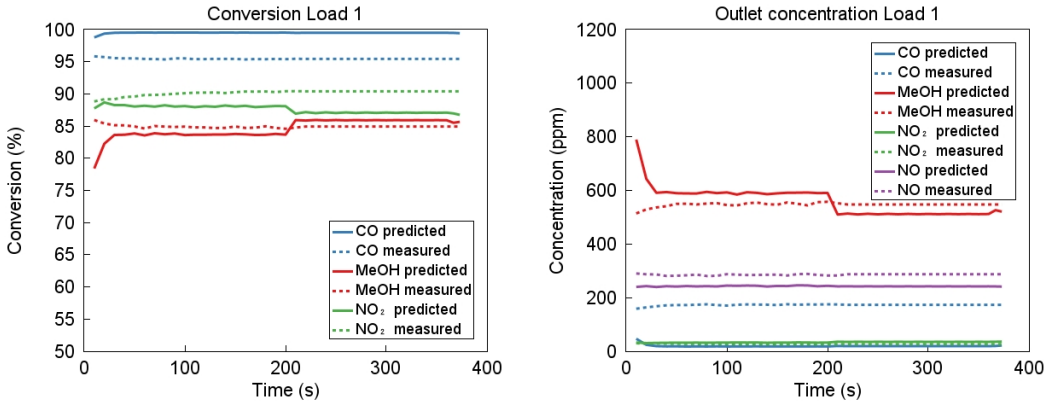

(a) Conversion **(b)** Outlet concentration

Figure A.6: The measured and predicted conversion and outlet concentration for Load 1.

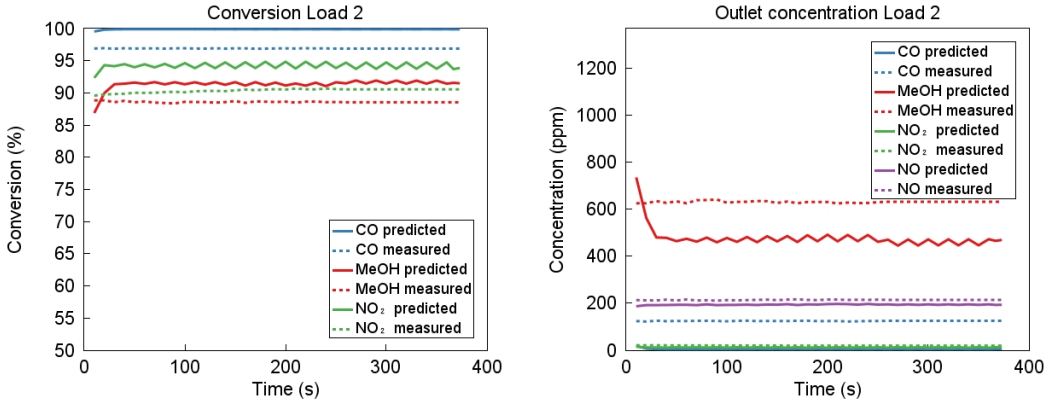

(a) Conversion **(b)** Outlet concentration

Figure A.7: The measured and predicted conversion and outlet concentration for Load 2.

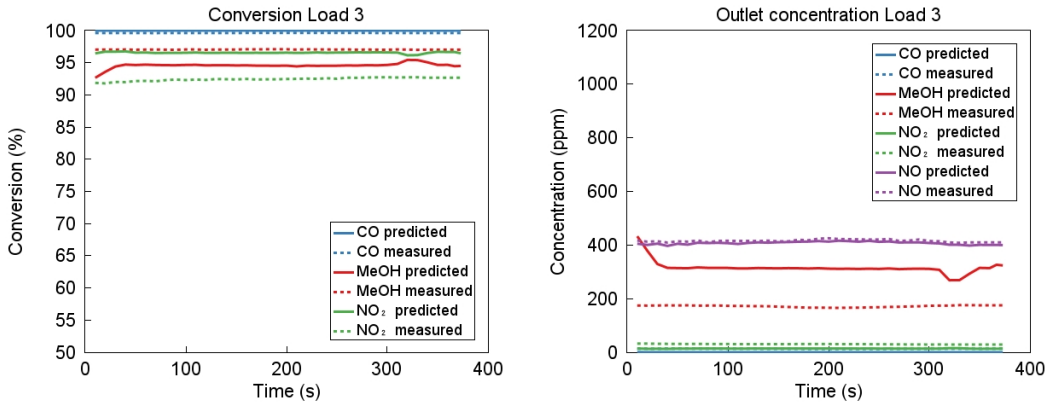

(a) Conversion **(b)** Outlet concentration

Figure A.8: The measured and predicted conversion and outlet concentration for Load 3.

Table A.2: Kinetic parameters for each reaction in the baseline model [1].

Reaction	**Pre-exponential factor** (A_i) **[-]**	**Activation energy** (E_{a_i}) **[J/mol]**
$CO + \frac{1}{2}\,O_2 \longrightarrow CO_2$	$1.183 \cdot 10^{12}$	81330
$NO + \frac{1}{2}\,O_2 \rightleftharpoons NO_2$	13270	6721
$MeOH + \frac{3}{2}\,O_2 \longrightarrow CO_2 + 2\,H_2O$	$1.566 \cdot 10^{19}$	159400
$CO + NO_2 \longrightarrow CO_2 + NO$	$1.183 \cdot 10^{12}$	81330
$MeOH + 3\,NO_2 \longrightarrow 3\,NO + 2\,H_2O + CO_2$	$1.566 \cdot 10^{19}$	159400

Table A.3: Optimized kinetic parameters for each reaction in the final model.

Reaction	**Pre-exponential factor** (A_i) **[-]**	**Activation energy** (E_{a_i}) **[J/mol]**
$CO + \frac{1}{2}\,O_2 \longrightarrow CO_2$	$5.99 \cdot 10^{12}$	89824
$NO + \frac{1}{2}\,O_2 \rightleftharpoons NO_2$	7080	28174
$MeOH + \frac{3}{2}\,O_2 \longrightarrow CO_2 + 2\,H_2O$	$1.01 \cdot 10^{9}$	53319
$CO + NO_2 \longrightarrow CO_2 + NO$	$2.46 \cdot 10^{10}$	49887
$MeOH + 3\,NO_2 \longrightarrow 3\,NO + 2\,H_2O + CO_2$	$2.27 \cdot 10^{12}$	104048

Table A.4: Optimized adsorption inhibition parameters for each species in the final model.

Species	**Pre-exponential factor** (A_{a_i}) [-]	**Activation energy**/R_g (E_{a_i}/R_g) [**K**]
CO	238.93	-1960.8
MeOH	560.92	-6428.0
NO	29348	-5072.4
NO equilibrium constant	0.016	838.46

DEPARTMENT OF CHEMISTRY AND CHEMICAL ENGINEERING
CHALMERS UNIVERSITY OF TECHNOLOGY
Gothenburg, Sweden
www.chalmers.se

CHALMERS
UNIVERSITY OF TECHNOLOGY